

1 Simulating the SOA formation of isoprene from partitioning 2 and aerosol phase reactions in the presence of inorganics

3
4 **R. L. Beardsley¹ and M. Jang^{1,*}**

5 [1]{Department of Environmental Engineering Sciences, University of Florida, P.O. Box
6 116450, Gainesville, FL 32611, USA }

7 Correspondence to: M. Jang (mjang@ufl.edu)

8 9 **Abstract**

10 The secondary organic aerosol (SOA) produced by the photooxidation of isoprene with and
11 without inorganic seed is simulated using the Unified Partitioning Aerosol Phase Reaction
12 (UNIPAR) model. Recent work has found the SOA formation of isoprene to be sensitive to
13 both aerosol acidity ($[H^+]$, mol/L) and aerosol liquid water content (LWC) with the presence
14 of either leading to significant aerosol phase organic mass generation and large growth in
15 SOA yields (Y_{SOA}). Classical partitioning models alone are insufficient to predict isoprene
16 SOA formation due to the high volatility of photooxidation products and sensitivity of their
17 mass yields to variations in inorganic aerosol composition. UNIPAR utilizes the chemical
18 structures provided by a near-explicit chemical mechanism to estimate the thermodynamic
19 properties of the gas phase products, which are lumped based on their calculated vapor
20 pressure (8 groups) and aerosol phase reactivity (6 groups). UNIPAR then determines the
21 SOA formation of each lumping group from both partitioning and aerosol phase reactions
22 (oligomerization, acid catalyzed reactions, and organosulfate formation) assuming a single
23 homogeneously mixed organic-inorganic phase as a function of inorganic composition and
24 VOC/NO_x. The model is validated using isoprene photooxidation experiments performed in
25 the dual, outdoor UF APHOR chambers. UNIPAR is able to predict the experimental SOA
26 formation of isoprene without seed, with H₂SO₄ seed gradually titrated by ammonia, and with
27 the acidic seed generated by SO₂ oxidation. Oligomeric mass is predicted to account for more
28 than 65% of the total OM formed in all cases and over 85% in the presence of strongly acidic
29 seed. The model is run to determine the sensitivity of Y_{SOA} to $[H^+]$, LWC, and VOC/NO_x, and
30 it is determined that the SOA formation of isoprene is most strongly related to $[H^+]$ but is

1 dynamically related to all three parameters. For $\text{VOC}/\text{NO}_x > 10$, with increasing NO_x both
2 experimental and simulated Y_{SOA} increase and are found to be more sensitive to $[\text{H}^+]$ and
3 LWC. For atmospherically relevant conditions, Y_{SOA} is found to be more than 150% higher in
4 partially titrated acidic seeds (NH_4HSO_4) than in effloresced inorganics or in isoprene only.

5

6 **1 Introduction**

7 Volatile organic compounds (VOCs) are emitted into the atmosphere from both biogenic and
8 anthropogenic sources. Once emitted, these compounds react with atmospheric oxidants and
9 radicals to form semi-volatile products that may self-nucleate or partition onto pre-existing
10 particulate matter to form secondary organic aerosol (SOA). Isoprene (2-methyl-1,3-
11 butadiene) is a biogenic VOC with the largest emission of all non-methane hydrocarbons
12 (Guenther et al., 2006), and yet it was initially thought to form insignificant amounts of SOA
13 due to the volatility of its principal oxidation products. This conclusion was supported by
14 early chamber investigations that found isoprene only forms SOA at concentrations much
15 higher than ambient conditions (Pandis et al., 1991; R. M. Kamens et al., 1982). However,
16 recent chamber (Edney et al., 2005; Kroll et al., 2005, 2006; Limbeck et al., 2003) and field
17 studies (Claeys et al., 2004; Edney et al., 2005) found that the large emission rate of isoprene
18 makes the contribution to global SOA formation significant even at low yields, and it is
19 estimated that isoprene is the largest single source of global organic aerosol (Henze and
20 Seinfeld, 2006). The proposal of new SOA formation mechanisms, primarily the classical
21 equilibrium partitioning theory by Pankow (1994) and the discovery of aerosol phase
22 oligomerization reactions in the presence of inorganic acids (Jang et al., 2002, 2003), led to
23 the re-examination of the SOA formation potential of isoprene. More recent studies have
24 found the SOA yield of isoprene and its oxidation products to be highly sensitive to aerosol
25 acidity ($[\text{H}^+]$, mol/L aerosol) (Jang et al., 2002; Kuwata et al., 2015; Limbeck et al., 2003;
26 Surratt et al., 2010) and aerosol liquid water content (LWC).

27 The tendency of isoprene photooxidation products to engage in aerosol phase oligomerization
28 reactions is primarily due to the reactivity of its secondary products. The presence of two
29 double bonds makes isoprene highly reactive and allows for rapid OH initiated oxidation in
30 the atmosphere. The distribution of isoprene photooxidation products and the resultant SOA
31 yields are dependent on NO_x concentrations and atmospheric aging. When NO_x
32 concentrations are low, RO_2 radicals react with HO_2 radicals to form hydroxyperoxides

1 (ROOH) at high yield. Then, ROOH further react with OH radicals to form
2 dihydroxyepoxides (IEPOX) (Paulot et al., 2009). IEPOX has been found to undergo rapid
3 reactive uptake onto wet ammonium sulfate (AS) inorganic aerosol and acidic inorganic seeds
4 at all RH leading to the formation of tetrols, organosulfates (OS) and other low volatility
5 oligomers. In the presence of high NO_x, SOA formation will depend on the ratio of NO₂ to
6 NO with isoprene SOA yields being be lower at low NO₂/NO due to RO₂ reacting with NO to
7 produce more volatile products (Kroll et al., 2006; Surratt et al., 2010).

8 In order to quantify and understand the impact of SOA on climate and human health, the
9 prediction of SOA formation of isoprene is essential. SOA models have been developed and
10 utilized to predict the SOA formation of various VOC systems. The two-product model was
11 developed based on classical partitioning theory (Pankow, 1994) and represents SOA
12 formation through use of two or more representative secondary products of varying vapor
13 pressure (Odum et al., 1996). By fitting the stoichiometric and partitioning coefficients of
14 each representative semi-volatile organic compound (SVOC) to experimental data, the SOA
15 yield of a VOC is predicted as a function of the absorbing organic mass (OM) concentration
16 without considering the numerous gas phase products. The simple and efficient handling of
17 SOA mass formation from partitioning by the two-product model led to its widespread use in
18 regional and global models. Nevertheless, the two-product model and its predecessors are
19 limited in their ability to predict SOA formation from aerosol phase reactions in the presence
20 of inorganic aerosol due to the loss of individual product structures, which determine
21 reactivity in the aerosol phase, and the need to fit new parameters for variations in
22 atmospheric conditions. Many regional models have already incorporated different sets of
23 parameters for each VOC under high and low NO_x regimes, but cannot handle the variations
24 seen in ambient aerosol LWC and [H⁺] that enhance SOA formation via aerosol phase
25 reactions (Carlton et al., 2009).

26 More recent studies have modeled aqueous phase SOA production using empirically
27 determined uptake coefficients or effective Henry's constants (when available) to estimate
28 reactive uptake of major isoprene products, such as IEPOX and glyoxal, in the inorganic
29 aqueous phase (Marais et al., 2016; McNeill et al., 2012; Pye et al., 2013; Woo and McNeill,
30 2015). For example, McNeill et al. (2012) developed the box model GAMMA to predict the
31 aqueous SOA production of isoprene in the presence of deliquesced ammonium sulfate. Pye
32 et al. (2013) modified the regional Community Multi-scale Air Quality model to include the

1 heterogeneous uptake of IEPOX and methacrylic acid epoxide. While these models greatly
2 improve the predictions of isoprene SOA formation over classical partitioning models, SOA
3 formation of these known products via aqueous phase reactions is not fully representative of
4 total isoprene SOA formation. Edney et al. (2005) measured the composition of isoprene SOA
5 in the presence of acidic inorganic seed, and methylglyceric acid and 2-methyltetrols, which
6 are tracer species for aqueous phase reactions, made up only 6% of the total SOA mass with
7 the majority of the products being unidentified. Furthermore, highly oxidized oligomers
8 comprise the majority of isoprene SOA even in the absence of an inorganic aqueous phase
9 (Nguyen et al., 2010; Surratt et al., 2006) due to aerosol phase reactions in organic-only
10 aerosol. The photooxidation of isoprene produces a large number of highly reactive products
11 (epoxides, carbonyls) that will react even in the absence of an inorganic aqueous phase to
12 produce the large fraction of high molecular weight (MW) species. Therefore, while the high
13 contribution of the aqueous phase products of IEPOX and similar compounds make them
14 ideal tracers, they are not fully representative of isoprene SOA as is demonstrated by the large
15 number of high MW products and lack of mass closure in isoprene composition studies even
16 in the absence of an inorganic aqueous phase.

17 In this study, the Unified Partitioning-Aerosol Phase Reaction (UNIPAR) model, which was
18 previously developed and applied to aromatic VOCs (Im et al., 2014), was updated and
19 expanded to model the SOA formation of isoprene in the presence of low VOC/NO_x (due to
20 the high sensitivity to [H⁺] in the low NO_x regime) and aerosol acidity using natural sunlight.
21 UNIPAR predicts SOA formation from gas-particle partitioning, and oligomerization
22 reactions in both organic-only aerosol and the inorganic aqueous phase using a lumping
23 structure that was developed to be representative of the thermodynamic properties and
24 chemical reactivity of oxidized products in the aerosol phase. The model was validated using
25 outdoor chamber data from isoprene photooxidation experiments with and without acidic
26 inorganic seeds.

27 **2 Experimental Methods**

28 Isoprene SOA photooxidation experiments were performed in the University of Florida
29 Atmospheric PHotochemical Outdoor Reactor (UF-APHOR) chambers over the period of a
30 day. The dual 52 m³ Teflon film chambers were operated simultaneously to allow for
31 investigation of two different experimental conditions under the same ambient, diurnal
32 profiles of sunlight, RH, and T. The chamber air was cleaned using air purifiers (GC Series,

1 IQAir) for 48 hours prior to each experiment. In the experiments in which inorganic seeds
2 were used, a 0.01 M aqueous solution of H₂SO₄ (SA) was atomized using a nebulizer (LC
3 STAR, Pari Respiratory Equipment) with clean air flow. Next, the desired volume of NO (2%
4 in N₂, Airgas) was injected into the chamber and finally, isoprene (99%, Sigma Aldrich) and
5 CCl₄ (>99.9%, Sigma Aldrich) were injected using a glass manifold with clean air. CCl₄ was
6 used as a tracer for dilution. All chemical species were injected early enough to allow for
7 stabilization and measurement before reactions begun with sunrise. The experimental
8 conditions for each of the chamber runs is shown in Table 1.

9 To allow for gas and aerosol phase characterization, chamber air is pumped through a number
10 of sampling lines into the lab that is located directly below the roof. Gas phase concentrations
11 of NO_x, O₃, and SO₂ were measured using a Teledyne Model 200E Chemiluminescence NO-
12 NO_x Analyzer, Model 400E Photometric O₃ Analyzer, and Model 102E Fluorescence TRS
13 Analyzer, respectively. A HP 5890 Gas Chromatography-Flame Ionization Detector was
14 employed with an oven temperature of 40 °C to measure isoprene and CCl₄ concentrations. A
15 semi-continuous OC/EC carbon aerosol analyzer (Sunset Laboratory, Model 4) following the
16 NIOSH 5040 method was utilized to measure organic carbon (OC) mass concentration (µgC
17 m⁻³), and then converted to OM using an OM/OC ratio of 2.2 (Aiken et al., 2008; Kleindienst
18 et al., 2007). Particle number and volume concentrations were measured with a scanning
19 mobility particle sizer coupled with a condensation nuclei counter (TSI, Model 3025A and
20 Model 3022). Particle wall loss was corrected using size-dependent first order rate constants
21 determined by a chamber characterization with inorganic seed.

22 A Particle into Liquid Sampler (Applikon, ADI 2081) coupled to Ion Chromatography
23 (Metrohm, 761Compact IC) (PILS-IC) was used to quantify aerosol phase inorganic ions. The
24 Colorimetry integrated with Reflectance UV-Visible spectrometer (C-RUV) technique (Jang
25 et al., 2008; Li et al., 2015; Li and Jang, 2012) was used to measure [H⁺] (mol L⁻¹ aerosol) in
26 experiment SA2. The C-RUV technique utilizes a dyed filter to collect aerosol and act as an
27 indicator for particle acidity. The change in color is measured using a UV-Visible
28 spectrometer in absorbance mode and allows for determination of [H⁺] using a calibration
29 curve. Then the amount of [SO₄²⁻] that forms organosulfates (OS) ([SO₄²⁻]_{OS}) is estimated by
30 comparing the actual particle [H⁺] measured by the C-RUV technique to the [H⁺] predicted
31 using the inorganic composition from PILS-IC by the inorganic thermodynamic model, E-
32 AIM II (Clegg et al., 1998). OS are reversible in the high temperature water droplets of the

1 PILS system and so the measured $[\text{SO}_4^{2-}]$ is the total sulfate including OS. Therefore, by
2 reducing the amount of $[\text{SO}_4^{2-}]$ input into E-AIM II until the predicted $[\text{H}^+]$ matches the actual
3 value measured by C-RUV, the amount of $[\text{SO}_4^{2-}]_{\text{OS}}$ can be estimated. A more detailed
4 explanation of the use of the C-RUV technique to estimate OS in SOA can be found in Li et
5 al. (2015). A more complete description of the experimental design and chamber operation
6 can be found in Im et al. (2014).

7 **3 Model Description**

8 UNIPAR simulates the SOA formation of the VOC/NO_x photooxidation products from both
9 partitioning and aerosol phase reactions. The photooxidation of the VOC is predicted
10 explicitly offline, and products are lumped using their volatility and reactivity in aerosol
11 phase reactions (Sect. 3.1). SOA formation is then predicted for the lumped species
12 dynamically as a function of the inorganic aerosol composition ($[\text{H}^+]$, LWC). The inputs of
13 the model are the consumption of isoprene (ΔISO), VOC/NO_x, the change in aerosol phase
14 sulfate ($\Delta[\text{SO}_4^{2-}]$) and ammonium ions (ΔNH_4^+), T and RH at each time step ($\Delta t = 3$ min).

15 The overall model schematic is shown in Fig. 1. In order to account for effects of inorganic
16 aerosol, isoprene SOA formation is approached in two ways: SOA formation in the presence
17 of deliquesced inorganic seed ($\text{SO}_4^{2-} > 0$ and $\text{RH} > \text{ERH}$), and either isoprene only ($\text{SO}_4^{2-} = 0$)
18 or effloresced inorganic seed ($\text{SO}_4^{2-} > 0$ and $\text{RH} < \text{ERH}$) (Sect. 3.2 and 3.3). First, the total
19 mass originating from ΔVOC in each Δt is split among the lumping groups ($i_{m,n}$) and
20 combined with the remaining gas phase concentrations from previous steps to get the total gas
21 phase concentration of each $i_{m,n}$ ($C_{g,i}$, $\mu\text{g m}^{-3}$) (Sect. 3.1). Then the concentrations in the
22 aerosol phase ($C_{\text{mix},i}$, $\mu\text{g m}^{-3}$) are calculated based on the aerosol phase state. Using the
23 estimated $C_{\text{mix},i}$ and inorganic aerosol composition, the OM formation from aerosol phase
24 reactions (OM_{AR} , $\mu\text{g m}^{-3}$) is calculated (Sect. 3.3.1). OM_{AR} includes SOA formation from
25 organic-only oligomerization reactions, aqueous phase reactions and acid-catalyzed reactions,
26 and OS formation (Sect. 3.3.2). OM_{AR} is assumed to be non-volatile and irreversible. Finally,
27 the OM from partitioning (OM_{P} , $\mu\text{g m}^{-3}$) is predicted using the module developed by Schell et
28 al. (2001) modified to account for the assumed non-volatility and irreversibility of OM_{AR}
29 (Sect. 3.3.3).

1 3.1 Gas phase photooxidation and lumping structure

2 The photooxidation of isoprene was simulated using the Master Chemical Mechanism v3.2
3 (Saunders et al., 1997, 2003) within the Morpho kinetic solver (Jeffries, H.E. et al., 1998).
4 Simulations were performed under varying VOC/NO_x ratios (ppbC/ppb) using the sunlight,
5 temperature, and RH data from 23 April 2014. All of the simulations began with NO and
6 begin with sunrise. The sunlight, RH, and temperature profiles used can be seen in the
7 supplemental information (SI) as well as an example gas phase simulation with corresponding
8 experimental data (Sect. S1).

9 The predicted photooxidation products are then lumped in UNIPAR using vapor pressure (m,
10 8 bins) and reactivity (n, 6 bins). The lumping structure is shown in Fig. S3 in the SI
11 including the structure of the product which contributes most to each lumping group. The
12 subcooled liquid vapor pressure of each product ($p^{\circ}_{L,i}$) is estimated using a group contribution
13 method (Joback and Reid, 1987; Stein and Brown, 1994; Zhao et al., 1999), which is
14 explained in detail in Im et al. (2014). The reactivity of each product is estimated based on the
15 number of reactive functional groups. The reactivity bins used in UNIPAR are very fast (VF,
16 α -hydroxybicycarbonyls and tricycarbonyls), fast (F, 2 epoxides or aldehydes,), medium (M, 1
17 epoxide or aldehyde), slow (S, ketones), partitioning only (P), and organosulfate precursors
18 (OS_P, 3 or more alcohols). The reactivity bins were developed based on previous work in
19 which the measured gas-particle partitioning coefficients (K_p) of toluene and α -pinene SOA
20 products were found to deviate from the theoretical value due to higher than expected particle
21 concentrations. The degree of deviation was found to depend on the functionalization of the
22 SOA product (Jang et al., 2002; Jang and Kamens, 2001). The experimental $\log(K_p)$ of
23 ketones (S reactivity bin) were found to be only slightly higher than the theoretical value,
24 while the experimental $\log(K_p)$ of conjugated aldehydes (M reactivity bin) and the products
25 associated with F and VF reactivity bins were found to be 10-40 times higher and 2 to 3
26 orders higher, respectively.

27 In order to account for their unique reactivity, glyoxal was allocated to group 6F instead of 8F
28 and methylglyoxal was moved from 8M to 6M based on their apparent Henry's constant (Ip et
29 al., 2009). In addition to these reactivity bins, isoprene required the designation of a medium
30 reactivity, multi-alcohol (M-OS_P) bin due to the large number of secondary products which
31 contain both three or more alcohols and reactive functional groups (epoxide or aldehyde).
32 Tetrol precursors (IEPOX), which are produced at high concentrations in the gas phase under

1 low VOC/NO_x, were also given a separate reactivity bin in order to more easily quantify the
2 SOA formation of these products predicted by the model. The concentrations of each lumping
3 group were set at the peak HO₂/NO ratio, which generally corresponds with the time of
4 majority of SOA formation and represents a shift from less oxidized to more oxidized
5 products. The corresponding stoichiometric mass coefficients (α_i) of each $i_{m,n}$ were then fit to
6 the initial VOC/NO_x ratio. At higher NO, it takes longer to reach the peak HO₂/NO ratio and
7 SOA formation is also slower. Fig. 2 shows the filled lumping structure at VOC/NO_x of 25
8 illustrating the high volatility and reactivity of the majority of isoprene products.

9 **3.2 Aerosol composition and phase state**

10 Tropospheric aerosols have been shown to be primarily composed organic compounds and
11 inorganic sulfate partially or wholly titrated with ammonia (Bertram et al., 2011; Murphy et
12 al., 2006). Under ambient diurnal patterns of RH, these aerosols may effloresce and
13 deliquesce, and can be liquid-liquid phase separated (LLPS) or a single homogeneously
14 mixed phase (SHMP) influencing the amount and composition of SOA formed. While dry,
15 effloresced inorganic salts simply act as a seed for organic coating by SOA, deliquesced seeds
16 contain liquid water into which reactive, soluble compounds can dissolve and further react
17 producing low volatility SOA (Hennigan et al., 2008; Lim et al., 2010; Volkamer et al., 2007).
18 Furthermore, the type of SOA products will determine the phase state of wet aerosol. In LLPS
19 aerosol, hydrophobic SVOC will partition primarily into the organic liquid phase, while a
20 significant fraction of hydrophilic SVOC may dissolve into the salted liquid phase. The RH at
21 which these transitions occur depends on the concentration and composition of the inorganic
22 and organic components of the aerosol.

23 Bertram et al. (2011) semi-empirically predicted the efflorescence RH (ERH), deliquescence
24 RH (DRH), and the RH of LLPS (SRH) by fitting experimental data of a number of
25 oxygenated organic-AS systems to the oxygen to carbon atomic ratio (O:C) and to the organic
26 to sulfur mass ratio (org:sulf) of the bulk aerosol. UNIPAR utilizes these parameterizations to
27 predict ERH and DRH at each time step ($t = j$) using modeled O:C and org:sulf from the
28 previous time step ($t = j - 1$). In regards to phase state, UNIPAR is run assuming a SHMP for
29 all of the isoprene simulations due to literature O:C values of isoprene ranging from 0.69 to
30 0.88 (Bertram et al., 2011; Chen et al., 2011; Kuwata et al., 2013), which corresponds to a
31 SRH of zero.

1 The interaction of organics and inorganics in SHMP SOA may alter the dissociation of
 2 inorganic acids and the resulting $[H^+]$ (mol L⁻¹ aerosol). In order to estimate the impact of
 3 organics on $[H^+]$ in SHMP isoprene SOA, the percent dissociation of H₂SO₄ was determined
 4 using AIOMFAC in the presence of varying amounts of tetrol and hexane, which represent
 5 polar and non-polar organic species, under controlled RH. The change in percent dissociation
 6 was less than 15% when compared to inorganic only aerosol at the same RH (details in
 7 supplemental information, Sect. S2). Based on these results, it was assumed that presence of
 8 organics in isoprene SHMP SOA does not significantly influence the $[H^+]$ from inorganic
 9 acids. Therefore, $[H^+]$ is estimated for each time step by E-AIM II (Clegg et al., 1998)
 10 corrected for the ammonia rich condition (Li and Jang, 2012) as a function of inorganic
 11 composition measured by PILS-IC ($[SO_4^{2-}]$, $[NH_4^+]$), and RH. Then, $[H^+]$ is diluted using the
 12 ratio of the inorganic volume to the total aerosol volume. The inorganic associated LWC is
 13 also calculated using E-AIM II. The LWC of isoprene SOA is estimated in AIOMFAC using
 14 the hygroscopic growth factor of a representative isoprene SOA: 20% sucrose by mass
 15 (Hodas et al., 2015) as a surrogate for tetrol and 80% isoprene derived oligomers (Nguyen et
 16 al., 2011). The estimated growth factor is approximately 30% of that of AS and so, in the
 17 model the LWC of isoprene is estimated to be 0.3 of the LWC of AS without an ERH. $[H^+]$ is
 18 used to describe particle acidity and has units of mol H⁺/L of aerosol. Therefore, $[H^+]$ will
 19 change with variation in inorganic composition, LWC and total aerosol mass (SOA). The
 20 particle pH is simply the negative log of $[H^+]$.

21 3.3 SOA formation

22 In simulating the total OM (OM_T) from isoprene photooxidation, UNIPAR predicts the SOA
 23 formation for each $i_{m,n}$ from both partitioning (OM_{P,i}) and aerosol phase reactions (OM_{AR,i}). In
 24 the previous applications of UNIPAR for aromatic VOC (Im et al., 2014), SOA formation
 25 was modeled under the assumption of LLPS aerosol because aromatic SOA is relatively non-
 26 polar, and thus aerosol phase concentrations of $i_{m,n}$ were calculated by means of a mass
 27 balance between the concentrations in the gas phase, the inorganic aerosol phase, and the
 28 organic aerosol phase. In modeling isoprene SOA formation in the presence of a SHMP
 29 aerosol, the total concentration (μg m⁻³ of air) of each lumping species ($C_{T,i}$) was split solely
 30 between $C_{g,i}$ and $C_{mix,i}$ by a single gas-particle partitioning coefficient, $K_{mix,i}$ (m³ μg⁻¹),

$$31 \quad C_{T,i} = C_{g,i} + C_{mix,i} \quad (1)$$

$$1 \quad K_{mix,i} = \frac{C_{mix,i}}{C_{g,i} M_{mix}}, \quad (2)$$

2 where M_{mix} is the total suspended matter and is the sum of the inorganic mass (M_{in}) and OM_T .
 3 Calculation of $K_{mix,i}$ follows the gas-particle absorption model (Pankow, 1994).

$$4 \quad K_{mix,i} = \frac{7.501 RT}{10^9 MW_{mix} \gamma_{mix,i} p_{L,i}^o}, \quad (3)$$

5 where R is the gas constant ($8.314 \text{ J K}^{-1} \text{ mol}^{-1}$), T is the temperature (K), MW_{mix} is the average
 6 molecular weight (g mol^{-1}) of the SHMP aerosol, $\gamma_{mix,i}$ is the activity coefficient of the
 7 lumping species in the SHMP aerosol, and $p_{L,i}^o$ is the sub-cooled liquid vapor pressure
 8 (mmHg) of $i_{m,n}$. $\gamma_{mix,i}$ accounts for the non-ideality in the SHMP aerosol and allows for more
 9 realistic representation of the differences in solubility in the aerosol phase. $\gamma_{mix,i}$ will vary
 10 between partitioning species due to differences in polarity and molar volume ($V_{mol,i}$), and also
 11 over time due to changes in LWC and aerosol composition.

12 In order to handle the range of possible $\gamma_{mix,i}$ in SHMP isoprene SOA, the AIOMFAC model
 13 was run using the highest concentration product of each $i_{m,n}$ (Fig. S3) in the presence of a
 14 mixed isoprene SOA/AS aerosol. The representative isoprene SOA composition was chosen
 15 based on the results of Nguyen et al. (2011). The bulk organic to sulfur mass ratio (*org:sulf*),
 16 concentration of $i_{m,n}$, and the RH were varied to cover the range of experimental values, and
 17 the resulting $\gamma_{mix,i}$ were fit to the bulk aerosol *org:sulf*, $\ln(RH)$, and the $V_{mol,i}$ and $O:C_i$ of each
 18 $i_{m,n}$ using a polynomial equation. The resulting parameterizations are shown in the SI along
 19 with the predicted $\gamma_{mix,i}$ plotted against $\gamma_{mix,i}$ from AIOMFAC (Sect. S4). In the absence of
 20 inorganic aerosol ($[\text{SO}_4^{2-}] = 0$) or in the presence of dry inorganic aerosol, partitioning is
 21 assumed to be ideal with organic only partitioning coefficient ($K_{or,i}$) calculated using $\gamma_{mix,i}$ of 1
 22 (Jang and Kamens, 1998) (Fig. 1).

23 **3.3.1 OM from aerosol phase reactions (OM_{AR})**

24 Once $C_{mix,i}$ ($\mu\text{g m}^{-3}$) is determined for each Δt , the OM_{AR} formation of $i_{m,n}$ is estimated in
 25 UNIPAR assuming a second-order self-dimerization reaction as is shown in Eq. 4,

$$26 \quad \frac{dC'_{mix,i}}{dt} = -k_{AR,i} C'_{mix,i}{}^2. \quad (4)$$

1 where $C_{\text{mix},i}^{\circ}$ is the aerosol phase concentration of $i_{m,n}$ in mol L⁻¹ of aerosol and $k_{AR,i}$ (L mol⁻¹ s⁻¹)
2 ¹) is the aerosol phase reaction rate of each $i_{m,n}$. $k_{AR,i}$ (Eq. 5) is calculated each time step using
3 the semi-empirical model developed by Jang et al. (2005) as a function of the reactivity, R
4 (VF, F, M, S; Sect. 3.1), and $\text{p}K_{\text{BH}^+}$ of $i_{m,n}$ in the aerosol phase, $[\text{H}^+]$ and LWC (activity of
5 water, a_w) from the inorganic thermodynamic model (Sect. 3.2), and the excess acidity, X (Im
6 et al., 2014; Jang et al., 2006).

$$7 \quad k_{AR,i} = 10^{(0.0005 * \text{p}K_{\text{BH}^+} + y * X + 1.3 * R + \log(a_w) + \log([\text{H}^+]) - 5.5)} \quad (5)$$

8 All of the coefficients of Eq. 5 were fit using the flow reactor experimental sets for aerosol
9 growth of model organic compounds (various aldehydes) on acidic aerosol ($\text{SO}_4^{2-} - \text{NH}_4^+ -$
10 H_2O) within the LLPS module and tested for LLPS aerosol (toluene SOA and 1,3,5-
11 trimethylbenzene SOA) by Im et al. (2014), except for the factor y for X . In the presence of
12 deliquesced inorganics, $k_{AR,i}$ is a function of X , which represents the effect of an acidic
13 inorganic medium on the reaction of the protonated organics that act as an intermediate for
14 acid-catalysed reactions. For LLPS aerosol, the protonated organic compounds are in highly
15 concentrated inorganic liquid with high X . The mixture of organic and inorganic species in
16 SHMP aerosol will lead to a modification of X and thus the reaction rate of protonated
17 organics. To account for this change in isoprene SOA, y was determined to be 0.49 by fitting
18 the OM_T of experimental set SA1 (Table 1). In the absence of deliquesced inorganic species,
19 the terms associated with the inorganic aqueous phase ($[\text{H}^+]$ and X) approach zero making
20 $k_{AR,i}$ primarily a function of the reactivity (R) of $i_{m,n}$ allowing for the prediction of
21 oligomerization reactions in the organic only aerosol.

22 Then by assuming that OM_{AR} is non-volatile and irreversible, $\Delta\text{OM}_{AR,i}$ can be calculated as the
23 reduction in $C_{T,i}$ for each time step. The full derivation of the equations used to predict OM_{AR}
24 is shown in the SI (Sect. S3).

25 **3.3.2 OS formation**

26 Sulfuric acid produced from the photooxidation of SO_2 influences aerosol phase state and
27 hygroscopicity (Sect. 3.2), and acts as a catalyst in OM_{AR} formation. It can be wholly or
28 partially titrated by ammonia, or it can react with reactive organic compounds to form OS.
29 The formation of OS from the esterification of $[\text{SO}_4^{2-}]$ with reactive organic functional groups
30 leads to a reduction in $[\text{H}^+]$ and LWC influencing subsequent OM_{AR} formation (Im et al.,
31 2014). Therefore, the formation of OS must be estimated in order to accurately predict SOA

1 growth. Of the total $[SO_4^{2-}]$ present in the SHMP aerosol, we assume that the sulfate which is
 2 not associated with ammonium ($[SO_4^{2-}]_{free}=[SO_4^{2-}]-0.5[NH_4^+]$) can form OS. The fraction of
 3 $[SO_4^{2-}]_{free}$ that forms OS is calculated using Eq. 6,

$$4 \frac{[SO_4^{2-}]_{OS}}{[SO_4^{2-}]_{free}} = 1 - \frac{1}{1 + f_{OS} \frac{N_{OS}}{[SO_4^{2-}]_{free}}}. \quad (6)$$

5 where f_{OS} is a semi empirical parameter determined to be 0.07 by Im et al. (2014) by fitting
 6 the $[H^+]$ predicted by UNIPAR to the measured $[H^+]$ in toluene SOA, as a measure of OS
 7 formation, using the method of Li et al. (2015). The experimentally determined f_{OS} was
 8 validated for isoprene SOA using the experimental data of this study (Sect. 4.1). N_{OS} is the
 9 number of OS forming functional groups present in the aerosol phase. The functional groups
 10 that have been shown to form OS are alcohols (Eddingsaas et al., 2012; Li et al., 2015;
 11 Minerath et al., 2008; Zhang et al., 2012), aldehydes (Liggio et al., 2005), and epoxides
 12 (Surratt et al., 2010). Alcohols and aldehydes can react with $[SO_4^{2-}]$ in a single position, while
 13 epoxides react with $[SO_4^{2-}]$ in two positions following ring opening in the aerosol phase. The
 14 average number of $[SO_4^{2-}]$ reaction positions is determined for each $i_{m,n}$, and then N_{OS} is
 15 calculated as the product of the molar concentration and the reaction positions of $i_{m,n}$. Finally,
 16 $[SO_4^{2-}]_{OS}$ is removed from $[SO_4^{2-}]_{free}$ so that LWC and $[H^+]$ can be recalculated for the next
 17 time step. As OS forms, both LWC and $[H^+]$ are reduced.

18 3.3.3 OM from partitioning (OM_P)

19 After OM_{AR} formation, OM_{P,i} is calculated using the module developed by Schell et al. (2001)
 20 modified to account for the assumed non-volatility and irreversibility of OM_{AR}. After OM_{AR}
 21 formation, the amount of the remaining $C_{T,i}$ of each lumping group that partitions between the
 22 gas and the SHMP aerosol is calculated as a function of the effective gas-phase saturation
 23 concentration of $i_{m,n}$ ($C_{g,i}^*=1/K_{mix,i}$) using a mass balance following Eq. 7,

$$24 \quad OM_{P,i} = \left[(C_{T,i} - OM_{AR,i}) - C_{g,i}^* \frac{\frac{C_{mix,i}}{MW_i}}{\sum_i \left(\frac{C_{mix,i}}{MW_i} + \frac{OM_{AR,i}}{MW_{oli,i}} \right) + OM_o} \right], \quad (7)$$

25 where MW_k and MW_{oli} are the molecular weight ($g \text{ mol}^{-1}$) of the lumping species and the
 26 dimer of the lumping species, respectively, and OM_o is the pre-existing organic mass ($mol \text{ m}^{-3}$)

3). The system of non-linear equations solved iteratively and the calculated $OM_{P,i}$ are summed to get the total OM_P for each Δt . Unlike when $i_{m,n}$ partitions into an organic only phase ($\gamma=1$), $\gamma_{mix,i}$ is used in calculating $C_{g,i}^*$ to account for the non-ideality of $i_{m,n}$ partitioning into the SHMP aerosol (Sect. 3.2). The remaining concentration ($C_{T,i} - OM_{AR,i}$) are passed to the next time step and combined with the newly formed $i_{m,n}$ ($\Delta VOC^* \alpha_i$).

4 Results and discussion

4.1 Model evaluation: SOA yield, O:C, and organosulfate formation

The ability of UNIPAR to simulate the SOA formation from isoprene photooxidation in the presence and absence of acidic inorganic seeds under low initial VOC/NO_x was determined through comparison of the simulated OM_T and experimental OM formation (OM_{exp}). All OM_{exp} were corrected for particle wall loss. Fig. 3 shows measured and predicted SOA formation in the presence and absence of SA at initial VOC/NO_x of ~17 for ISO1 and SA1 and 32 for ISO2 and SA2. The experiments performed in the absence of inorganic seed (ISO1 and ISO2) are used to test the prediction of organic-only oligomerization by UNIPAR. SOA formation is reasonably predicted in the absence of an inorganic aqueous phase for both experimental conditions with a maximum SOA yield ($Y_{SOA} = \Delta OM_{exp} / \Delta Iso$) of 0.025 and 0.007 for ISO1 and ISO2, respectively. These SOA yields are similar to those of reported literature values for isoprene in the absence of acidic seeds (Dommen et al., 2006). The model marginally overestimates the SOA formation in beginning of each chamber run, but the modeled OM_T falls within the range of error of OM_{exp} once the rate of SOA formation stabilizes and reaches a maximum. OM_{AR} makes up the majority of OM_T (>65% in ISO1 and ISO2). This is in agreement with the work of Nguyen et al. (2010) and Surratt et al. (2006) who analyzed the composition of isoprene SOA formed in the absence of an inorganic aqueous phase and found that the majority of SOA mass was from oligomeric structures. Furthermore, UNIPAR predicts that the approximately 70% of the OM_T is from lumping group 3OS_p-M, of which more than 93% of the mass contribution is organic peroxides (MCM products C510OOH (~40%), C57OOH (~27%), C58OOH (~15%) and HMACROOH(11%), structures shown in Fig. S7 of the SI). This is close to the measurements of Surratt et al. (2006), in which 61% of the total mass in the absence of seeds is from organic peroxides.

The presence of SA seeds (shown in orange in Fig. 3) greatly increases yields under both experimental conditions resulting in Y_{SOA} of 0.085 and 0.048 for SA1 and SA2, respectively,

1 due to the dissolution of $i_{m,n}$ into a larger M_{mix} resulting from increased LWC and increased
2 $k_{AR,i}$ attributed to lower particle pH (higher $[H^+]$). Using the factor y that was fit using exp.
3 SA1 in Table 1 (Eq. 5 in Sect 3.3.1), the model accurately predicts the OM_T of exp. SA2 at a
4 lower VOC/ NO_x in the presence of SA seed. Overall, OM_{AR} is the dominant contributor to
5 OM_T for both sets contributing more than 65% and 85% in the absence and presence of SA,
6 respectively. Also, the higher VOC/ NO_x (lower NO_x) of both ISO2 and SA2 resulted in lower
7 Y_{SOA} than ISO1 and SA1 which is discussed further in Sect. 4.3. In experiment SO2 (Table
8 1), $SO_2(g)$ was introduced to the chamber instead of SA seed so that the model could be
9 further tested under a situation more representative on the ambient atmosphere in which SO_2
10 is oxidized to SA. As can be seen in Fig 3. (shown in green), the model also reasonably
11 predicts the OM_T .

12 In addition to OM_T , O:C and $[SO_4^{2-}]_{OS}$ were also predicted using the model. The predicted
13 $[SO_4^{2-}]_{OS}$ is important due to the consumption of SO_4^{2-} that leads to an increase in particle pH
14 and a reduction in LWC. In exp. SA2, $[SO_4^{2-}]_{OS}$ was measured using the C-RUV method
15 allowing for comparison to the model (refer to Sect. 2 for C-RUV method description). Fig. 4
16 shows time series of the model predicted and measured $[SO_4^{2-}]_{OS}$ along with the total $[SO_4^{2-}]$
17 and $[NH_4^+]$ measured by the PILS-IC, the measured RH, and the predicted particle pH. Once
18 SOA formation starts, OS quickly forms. The measured $[SO_4^{2-}]_{OS}$ is reasonably well predicted
19 by the model with the predicted value being within the range of error once SOA mass
20 stabilizes. The predicted pH is relatively stable in the first hour of the experiment because the
21 effects of decreasing RH (and LWC) and increasing $[NH_4^+]$ counteract each other, but once
22 SOA formation starts pH increases rapidly due to titration by NH_3 produced from the chamber
23 walls, the consumption of $[SO_4^{2-}]$ by OS formation, and the dilution of $[H^+]$ by SOA mass.
24 Overall, the predicted pH starts at -0.73 and increases to 0.65 at the end of the experimental
25 run, which is within the range of ambient aerosol pH measured by Guo et al. (2015) in the
26 S.E. U.S (mean: 0.94, min: -0.94, max: 2.23).

27 While the O:C of the experimental SOA were not measured, the simulated O:C can be
28 compared to literature values which range from 0.69 to 0.88 (Bertram et al., 2011; Chen et al.,
29 2011; Kuwata et al., 2013). UNIPAR estimates the O:C ratio using $O:C_i$ and mole fraction of
30 each species in the aerosol phase not accounting for changes that may result from
31 oligomerization, hydration or OS formation. In the presence of untitrated SA, the modeled
32 O:C is 0.69 which is the lower end of the range of literature values. With increasing titration

1 changes in composition lead to higher overall predicted O:C. In SA1, SA is partially titrated
2 by NH_3^+ over the course of the experiment and the resulting O:C is 0.84. For ISO1 and ISO2,
3 the O:C are 0.92 and 0.98, which is higher than the reported values. This is due to the
4 predicted SOA being comprised of a few compounds with O:C near 1 without considering the
5 change of molecular structures via aerosol phase reactions. Chen et al. (2011) showed a
6 similar result in that the O:C ratio of monomeric products in isoprene SOA is higher than that of
7 oligomers.

8 **4.2 Isoprene SOA yield and the influence of VOC/NO_x and inorganic** 9 **composition**

10 In the following sections the model is used to investigate the influence of VOC/NO_x, LWC,
11 and [H⁺] on isoprene Y_{SOA} and composition. The experimental conditions of SA1 (RH, T,
12 Δ ISO) are used in all of these simulations unless otherwise specified.

13 Recent studies have investigated the effect of NO_x on the SOA formation of isoprene for the
14 high NO_x regime (VOC/NO_x < 5.5) and in the absence of NO_x (Chan et al., 2010a; Kroll et
15 al., 2006; Xu et al., 2014), and found that in the Y_{SOA} of isoprene is non-linearly related to
16 VOC/NO_x with Y_{SOA} being highest at intermediate NO_x conditions (VOC/NO_x = ~2).
17 However, very little investigation has been performed on isoprene SOA formation within the
18 low NO_x regime (VOC/NO_x > 5.5 and NO_x > 0 ppb) of this study, which is typical of rural
19 areas downwind of urban centers (Finlayson-Pitts and Pitts, Jr., 1993). To investigate the
20 influence of the NO_x level on Y_{SOA} in this range, simulations were performed in which the
21 VOC/NO_x ratio was increased incrementally from 10 to 100 with SA seeded SOA without
22 titration and isoprene only SOA. The Y_{SOA} of each simulation are plotted in Fig. 5. Overall,
23 increasing NO_x within this range (decreasing VOC/NO_x) increases Y_{SOA} both with and without
24 acidic seeds, which agrees with the general trend of Kroll et al. (2006) where intermediate
25 NO_x conditions had higher Y_{SOA} than no-NO_x conditions. However, the degree of the increase
26 in Y_{SOA} with increasing NO_x is different for the isoprene only SOA and the SOA formed in the
27 presence of SA seeds, which has not previously been shown to the best of our knowledge.

28 Y_{SOA} increases much more rapidly with increasing NO_x in the presence of SA seeds, which is
29 due to an increase in the relative contribution of reactive species. RO radicals produced from
30 the reaction of RO₂ radicals with NO can lead to multifunctional carbonyls via reaction with
31 oxygen and also simple carbonyls such as glyoxal and methylglyoxal through fragmentation

1 of RO radicals. These products are all highly reactive in the aerosol phase and produce OM_{AR} .
2 Furthermore, some late generation RO_2 radicals, whose precursors are formed from the RO
3 pathway (High NO), react with HO_2 to form low volatility organic peroxides with alcohol
4 functional groups and an aldehyde (3OS_p-M: C510OOH, C570OOH, C580OOH, HMACROOH
5 in MCM, Sect S7). Therefore, increases in NO_x within the simulation condition (VOC/NO_x
6 10~100) of this study leads to increases Y_{SOA} with higher sensitivity to VOC/NO_x in the
7 presence of inorganic seed. Fig. S5 shows the stoichiometric mass coefficients (α_i) of
8 important products as a function of VOC/NO_x .

9 Y_{SOA} is also dynamically related to inorganic compositions. SOA formation in the absence of
10 inorganic seed is primarily a function of the characteristics of $i_{m,n}$ and the impact of LWC on
11 isoprene SOA is minimal. However, under ambient conditions SOA will typically be formed
12 in the presence of inorganic aerosol. Variations in the inorganic aerosol composition ($[SO_4^{2-}]$
13 and $[NH_4^+]$) and RH lead to significant changes in LWC and pH. At high LWC, the total
14 volume of absorptive mass (M_{mix}) increases allowing for hydrophilic $i_{m,n}$ to partition into the
15 aerosol in significant amounts and engage in aerosol phase reaction. Additionally, highly
16 reactive species such as IEPOX will react to rapidly form SOA in the presence of $[H^+]$
17 (Gaston et al., 2014). In Fig 6 the simulated Y_{SOA} is plotted as a function of the fractional free
18 sulfate (FFS), $([SO_4^{2-}]-0.5[NH_4^+])/[SO_4^{2-}]$, and RH. Unlike pH, which is very difficult to
19 measure, $[SO_4^{2-}]$, $[NH_4^+]$, and RH data are widely available and easy to measure, which is
20 why FFS and RH were used in Fig 6. Using an ion balance such as FFS alone has been shown
21 to be not representative of actual particle pH (Guo et al., 2015), but providing both FFS and
22 RH allow for estimation of pH within an inorganic thermodynamic model and ease of use by
23 future studies.

24 It is difficult to decouple the effects of $[SO_4^{2-}]$, LWC and pH since $[SO_4^{2-}]$ ultimately
25 influences both LWC and pH, but Fig 6 can be used to help elucidate the influence of these
26 effects in UNIPAR. For AS seed (FFS=0.0), SO_4 is entirely titrated by ammonia and the
27 lowest Y_{SOA} occurs below the ERH. As the RH increases, AS becomes deliquesced and the
28 LWC gradually rises leading to an increase in Y_{SOA} . This is true for the predictions at all small
29 values of FFS due to the increase in the total volume of absorptive mass (M_{mix}) associated
30 with increasing LWC, allowing for hydrophilic $i_{m,n}$ to partition into the aerosol in significant
31 amounts and engage in aerosol phase reactions. However, as the amount of $[NH_4^+]$ decreases
32 (FFS < 0.7, highly acidic), the effect of increasing LWC reverses, and Y_{SOA} decreases with

1 increasing LWC due to the dilution of $[\text{SO}_4^{2-}]$ and the resulting increase in pH. If RH is held
2 constant, varying FFS allows for investigation of the effect of pH on Y_{SOA} . Increasing FFS or
3 decreasing pH at constant RH leads to a rapid increase in Y_{SOA} at all RH due to an increase in
4 the SOA formation from the acid catalyzed reactions of species such as IEPOX. Therefore,
5 $[\text{SO}_4^{2-}]$ modulates Y_{SOA} within UNIPAR by controlling LWC and $[\text{H}^+]$ which influence $k_{\text{AR},i}$
6 (Eq. 5). The consumption of $[\text{SO}_4^{2-}]$ by OS formation is accounted for in UNIPAR through a
7 reduction in acidity and LWC, but the role of $[\text{SO}_4^{2-}]$ in reactive uptake as a nucleophile is not
8 directly accounted for.

9 **4.3 Simulated composition of isoprene SOA**

10 Analysis of the contributions of each $i_{m,n}$ to the overall OM_T allows for a determination of the
11 species that are significant in isoprene SOA for various inorganic compositions. Four
12 simulations were performed at 60% RH with AS and SA seeds at org:sulf of 0.5 and 1.5 to
13 capture the differences in composition as a result of changes in LWC, $[\text{H}^+]$, and M_{mix} .

14 The aerosol mass fraction of each $i_{m,n}$ (MF_i) under the simulated conditions are shown in Fig
15 7. IEPOX has been demonstrated to be an important precursor to ambient (Budisulistiorini et
16 al., 2015; Chan et al., 2010b) and laboratory generated (Lin et al., 2012; Paulot et al., 2009)
17 isoprene SOA leading to the formation of 2-methyltetrols (Surratt et al., 2010), OS (Liao et
18 al., 2015), and other species through aerosol phase reactions in which IEPOX products
19 contribute up to 33% of ambient OM in Southeast U.S. (Budisulistiorini et al., 2013). The
20 formation of IEPOX derived SOA has been shown to be primarily from the reactive uptake in
21 the presence of LWC and $[\text{H}^+]$, but is most highly correlated with aerosol acidity (Gaston et
22 al., 2014). In Fig. 7, it can be seen that the MF_i of IEPOX derived SOA is higher in the
23 presence of $[\text{H}^+]$. When accounting for the yield of each system, the total formation of IEPOX
24 derived SOA is much greater in the presence of SA seed than AS seed. Additionally, the MF_i
25 of IEPOX derived SOA falls within the range measured in literature. When org:sulf increases
26 from 0.5 to 1.5 in the presence of SA, the reduction of MF_i of IEPOX products is due to the
27 increasing contribution of other $i_{m,n}$ (7MA and OTHER) while the mass contribution of
28 IEPOX remains similar. The MF_i of glyoxal (GLY) is significant for all four simulations, but
29 increases with growth of M_{mix} due to its high aqueous solubility and tendency to form
30 hydrates that can form oligomers.

1 In the absence of acidity, $k_{AR,i}$ are relatively small and the MF_i are primarily a function of the
2 gas phase concentration, volatility and solubility of i . For example, in the AS seeded SOA
3 simulations, 3OS_p-M (organic peroxides with both an aldehyde and alcohols, Figures S3 and
4 S7) contributes more than half of the total mass (Fig. 7) due to its high gas phase
5 concentration and low volatility. As LWC and $k_{AR,i}$ increase (AS to SA seed aerosol and
6 org:sulf 1.5 to 0.5), more volatile and reactive $i_{m,n}$ are able to contribute to MF_i . Therefore, the
7 MF_i of 3OS_p-M is significantly reduced in SA seeded SOA as other $i_{m,n}$ contribute in larger
8 fractions. Overall, OM_P only contributes a small fraction of the total OM_T, and the MF_i of the
9 partitioning species generally decreases with increasing contribution of other species at higher
10 LWC and $[H^+]$.

11 **4.4 Model sensitivity, uncertainty, and limitations**

12 UNIPAR utilizes the chemical structures provided by MCM to estimate the thermodynamic
13 properties of the gas phase products, which are lumped based on their calculated vapor
14 pressure (8 groups) and aerosol phase reactivity (6 groups). However, since not all
15 atmospheric reactions have been studied in detail, MCM determines the products and kinetics
16 of unstudied reactions using the known degradation mechanisms of similar chemical species.
17 Pinho et al. (2005) evaluated the isoprene mechanism of MCM v3 by comparing the oxidation
18 of isoprene and its products methacrolein and methylvinyl ketone to chamber data. The model
19 performed reasonably well for these limited products, but a large amount of uncertainty
20 remains in regards to the prediction of the hundreds of other isoprene derived products.
21 Furthermore, the lumping approach of UNIPAR uses a fixed gas phase composition set at the
22 maximum HO₂/NO for each VOC/NO_x ratio. This approach does not account for changes to
23 the gas phase composition that occur due to continued oxidation.

24 Deviation of the estimated $p^{\circ}_{L,i}$ from the actual $p^{\circ}_{L,i}$ due to the uncertainty of the group
25 contribution method (Sect. 3.1) can change the lumping assignment affecting both OM_P and
26 OM_{AR}. The uncertainty associated with the group contribution method used for $p^{\circ}_{L,i}$
27 estimation is a factor of 1.45 (Joback and Reid, 1987; Stein and Brown, 1994; Zhao et al.,
28 1999). The temperature dependency of each lumping group as is calculated as a function of
29 the enthalpy of vaporization (ΔH_{vap}) and also has associated uncertainty that can affect the
30 model prediction. The error of this method is 2.6% (Kolská et al., 2005). To determine the
31 model sensitivity to these parameters, simulations of SA1 were performed by increasing and
32 decreasing $p^{\circ}_{L,i}$ and ΔH_{vap} by a factor of 1.5 and 1.1, respectively. The change in OM_T from

1 the baseline for each simulation is shown in Fig. S6. Increasing and decreasing $p_{L,i}^{\circ}$ by a
2 factor of 1.5 results in a 32.03% and -26.41% change, respectively, while modifying ΔH_{vap}
3 only leads to $\pm 0.27\%$ change.

4 The thermodynamic model AIOMFAC was employed to generate a simplified
5 parameterization to estimate $\gamma_{\text{mix},i}$ in the SHMP isoprene SOA as a function of O:C, org:sulf,
6 RH, and V_{mol} . AIOMFAC is a valuable tool for predicting the activity coefficients of complex
7 mixtures, but it has substantial uncertainty resulting from limitations of the database used in
8 development and the error associated with the underlying modules. Moreover, the expected
9 accuracy is limited further by the regression performed in UNIPAR. For the condition
10 simulated by UNIPAR, $\gamma_{\text{mix},i}$ are all near unity (0.65-1.75). Considering the characteristics of a
11 SHMP aerosol, a factor of 1.5 was applied to the predicted $\gamma_{\text{mix},i}$ and the resulting change in
12 OM_T is -16.22%/+32.00% (Fig S6), which is similar to the model sensitivity to $p_{L,i}^{\circ}$.

13 The other parameter largely affecting the simulated SOA formation in UNIPAR is $k_{AR,i}$, which
14 is calculated primarily as a function of LWC, $[\text{H}^+]$, and reactivity of $i_{m,n}$ (Sect. 3.3.1).
15 Estimations of LWC and $[\text{H}^+]$ are performed by the inorganic thermodynamic model E-AIM.
16 Similar to AIOMFAC, the accuracy of E-AIM will depend on the underlying assumptions and
17 the database used in development. For LWC, the predictions of E-AIM are consistent with
18 other inorganic thermodynamic models and are based on widely used, critically reviewed
19 water activity data (Zhang et al., 2000). However, inorganic thermodynamic models vary
20 widely in predicting $[\text{H}^+]$ especially at low RH. This is especially true for ammonia rich
21 inorganic salts at low RH. Corrections for the ammonia rich predictions of $[\text{H}^+]$ were applied
22 based on the results of Li and Jang (2012) in which aerosol $[\text{H}^+]$ was measured using a filter
23 based colorimetry method coupled with a PILS-IC. The total uncertainty of this method is
24 approximately 18%. There is also uncertainty stemming from the flow chamber study that
25 was used to fit the coefficients used in predicting $k_{AR,i}$. To determine the possible sensitivity of
26 the model to the combined uncertainty of the corrected E-AIM and the function used to
27 predict $k_{AR,i}$, a factor of 2.0 was applied to simulations and the resulting change in OM_T is
28 approximately $\pm 13\%$ (Fig S6).

29 Furthermore, not all recent advancements in the understanding of SOA formation mechanisms
30 are accounted for by UNIPAR, including but not limited to SOA viscosity, nighttime
31 chemistry of nitrate radicals (NO_3^*), and SVOC wall loss. Virtanen et al. (2010) reported that
32 biogenic SOA can exist as amorphous solids or glassy state, which can lead to deviations

1 from equilibrium processes, but Song et al. (2015) found that isoprene derived SOA is of low
2 viscosity under the range of ambient RH. Thus, impact of viscosity on isoprene SOA is
3 minimal. The nighttime reaction of isoprene with NO_3^* has been found to lead to significant
4 SOA formation due to the formation of stable primary organonitrate (ON). Ng et al. (2008)
5 measured SOA yields up to 23.8% from the dark chamber reaction of isoprene and NO_3^*
6 under dry conditions ($<10\%$ RH), while Rollins et al. (2012) linked NO_3^* chemistry to
7 ambient, nighttime SOA production with 27 to 40% of nighttime OM growth from ON.
8 Under low NO_x conditions, isoprene photooxidation has been shown to produce primarily
9 tertiary ON in both the gas phase and through aerosol phase epoxide reactions (Eddingsaas et
10 al., 2010; Paulot et al., 2009). Darer et al. (2011) investigated the stability of primary and
11 tertiary ON and found the tertiary ON to be highly unstable and to rapidly convert to OS and
12 polyols in both neutral and acidic SOA. Therefore, it is unlikely that ON significantly
13 contribute to the SOA investigated and modeled in this study.

14 A number of recent studies have found that the loss of gas phase vapors to chamber walls can
15 compete with gas-particle partitioning (Matsunaga and Ziemann, 2010; Zhang et al., 2014,
16 2015). Vapor wall loss was not accounted for in this study and thus the experimental SOA
17 mass may be low biased. However, based on the conclusions of Zhang et al. (2015), the high
18 volatility of isoprene products likely results in gas-particle partitioning outcompeting vapor
19 wall loss in chambers with a large ratio of volume to surface area.

20 Another new development in the SOA formation is the discovery of the salting-in and salting-
21 out of glyoxal and methylglyoxal (Waxman et al., 2015). While these effects are very
22 interesting and likely influence the SOA formation of these species, they are not yet included
23 within UNIPAR. The topic will be reconsidered for application within our model once these
24 effects have been more comprehensively investigated for a wider range of relevant water-
25 soluble organic molecules and inorganic aerosol compositions.

26 In the recent Southern Oxidant and Aerosol Study field campaign, Budisulistiorini et al.
27 (2015) and Xu et al. (2015) found ambient isoprene SOA formation in the SE U.S. to be most
28 highly correlated with $[\text{SO}_4^{2-}]$, and insensitive to $[\text{H}^+]$ and LWC. However, in the summer
29 months the aerosol of the SE U.S. are highly acidic (pH -1 to 2) and high in LWC due to the
30 high RH ($> 50\%$) (Guo et al., 2015). Under these conditions, the formation of isoprene
31 derived SOA is not likely to be highly correlated with changes in LWC and $[\text{H}^+]$ since both
32 are always high. Yet when comparing neutral and acidic conditions, the presence of acidity

1 has repeatedly been shown to lead to increases in Y_{SOA} (Lin et al., 2012; Surratt et al., 2007).
2 Most recently, Lewandowski et al. (2015) found up to a 459% increases in Y_{SOA} from the
3 presence inorganic acid $[H^+]$. Additionally, Xu et al. (2015) found a reduction in isoprene
4 derived SOA with increases RH for the highly acidic aerosol of the campaign. A similar
5 reduction with increasing RH is seen at high FFS in Fig. 6 due to the dilution of $[SO_4^{2-}]$ and
6 the corresponding $[H^+]$ by increases in LWC.

7 **5 Conclusions and Atmospheric Implications**

8 Under the assumption of SHMP aerosol, UNIPAR was able to simulate the low NO_x SOA
9 formation of isoprene from partitioning and aerosol phase reactions with and without an
10 inorganic acid seed. The data used to validate the model was generated using the UF-APHOR
11 outdoor chamber, which allows for day long experiments under ambient sunlight, T and RH.
12 For the SOA formation of isoprene in the absence of deliquesced inorganic seeds, UNIPAR
13 was able to predict the experimental OM_T using the same approach that was applied to
14 anthropogenic, aromatic VOCs in Im et al. (2014) without any modification. Differences
15 between the SHMP SOA formed by isoprene in the presence of deliquesced inorganic seeds
16 and LLPS SOA of the previous study required a slight reduction in $k_{AR,i}$. After validating the
17 model using the measured SOA formation of outdoor chamber experiments, simulations were
18 performed to elucidate the sensitivity of Y_{SOA} and composition to model parameters. From this
19 analysis it was determined that the Y_{SOA} of isoprene and the resulting SOA composition is
20 primarily a function of VOC/NO_x , $[H^+]$, and LWC. For the range of VOC/NO_x investigated
21 in this study (≥ 10), increases in NO_x corresponded with increases in Y_{SOA} and a higher
22 sensitivity to $[H^+]$. This is due to the increased production of highly reactive carbonyls, such
23 as glyoxal, and a more general shift to lower volatility (Figure S6).

24 Changes in $[H^+]$ and LWC were shown to strongly influence Y_{SOA} (Fig 6). At a given RH,
25 increases in $[H^+]$ result in increased OM formation. For titrated acidic aerosol, increases in
26 RH lead to gradual increases in Y_{SOA} . However for highly acidic aerosol ($FFS \geq 0.75$), increases
27 in RH decrease Y_{SOA} due to dilution of $[H^+]$. Overall, isoprene SOA formation was found to
28 be most sensitive to $[H^+]$ with the highest Y_{SOA} occurring at high FFS and low RH.

29 Due to the pervasiveness of isoprene in the ambient atmosphere, any variation in Y_{SOA} will
30 have a strong influence on the global SOA budget and needs to be accounted for by climate
31 and air quality models. Since the experimental runs and simulations performed in this study
32 were at concentrations beyond those of the ambient atmosphere, additional simulations were

1 performed to estimate Y_{SOA} for conditions more representative of the ambient atmosphere. The
2 ΔISO during each Δt was assumed to be constant and estimated assuming a pseudo first order
3 reaction with OH using an isoprene concentration of 2.4 ppb from the rural measurements of
4 Wiedinmyer et al. (2001) and a OH concentration of $1.0E6$ molecules/cm³. Using a $[SO_4^{2-}]$ of
5 $5.55 \mu\text{g}/\text{m}^3$ and OM_o of $3 \mu\text{g}/\text{m}^3$ based on the non-urban continental composition of
6 submicron PM from the review of Heintzenberg (1989), two sets of simulations were
7 performed for AS and AHS at RH of 30% and 60% and $VOC/NO_x=10$. The simulated Y_{SOA} of
8 AS are 0.01695 ($OM_T = 0.329 \mu\text{g m}^{-3}$) and 0.0207 ($OM_T = 0.402 \mu\text{g m}^{-3}$), and of AHS are
9 0.0446 ($OM_T = 0.867 \mu\text{g m}^{-3}$) and 0.0449 ($OM_T = 0.873 \mu\text{g m}^{-3}$) at 30% and 60% RH,
10 respectively. The OM_T formation and associated Y_{SOA} were calculated after an eight hour
11 simulation. AS at 30% RH is seen as the baseline as it is below the ERH. Increasing the
12 RH to 60% leads to a 22% increase in Y_{SOA} for AS due to the increased LWC. The presence of
13 AHS seeds and the resultant increase in $[H^+]$ leads to an increase of 163% and 165% in Y_{SOA}
14 over the baseline at 30% and 60% RH, respectively. These results support the conclusion that
15 the SOA formation of isoprene is more sensitive to $[H^+]$ than to LWC, but dynamically
16 related to both. Furthermore, while the SOA formation of isoprene may be reasonably
17 predicted as a linear function of $[H^+]$ for a specific RH and VOC/NO_x , as is proposed by
18 Surratt et al. (2007), a single linear relationship will not hold at different RH for a single
19 VOC/NO_x or under the possible range of conditions in the ambient atmosphere. In the
20 application of UNIPAR to the aromatic LLPS SOA system, Im et al. (2014) found the Y_{SOA} of
21 toluene to be higher in the presence AHS than AS at 30% RH, but the same at 60% RH
22 meaning that the SOA formation of toluene is less sensitive to $[H^+]$ but more sensitive to
23 LWC than isoprene. The relationship between Y_{SOA} , LWC, and $[H^+]$ will not only vary
24 dynamically for different VOC/NO_x but also between different VOC systems. Failure to
25 account for these relationships in regional and global scale models may lead to significant
26 underestimation of SOA formation in acidic and humid conditions.

27 **Acknowledgements**

28 This work was supported by the grant from the National Science Foundation (ATM-0852747)
29 and the grant from the National Research Funding of Korea (2014M3C8A5032316).

30

1 **References**

- 2 Aiken, A. C., DeCarlo, P. F., Kroll, J. H., Worsnop, D. R., Huffman, J. A., Docherty, K. S.,
3 Ulbrich, I. M., Mohr, C., Kimmel, J. R., Sueper, D., Sun, Y., Zhang, Q., Trimborn, A.,
4 Northway, M., Ziemann, P. J., Canagaratna, M. R., Onasch, T. B., Alfarra, M. R., Prevot, A.
5 S. H., Dommen, J., Duplissy, J., Metzger, A., Baltensperger, U. and Jimenez, J. L.: O/C and
6 OM/OC Ratios of Primary, Secondary, and Ambient Organic Aerosols with High-Resolution
7 Time-of-Flight Aerosol Mass Spectrometry, *Environ. Sci. Technol.*, 42(12), 4478–4485,
8 doi:10.1021/es703009q, 2008.
- 9 Bertram, A. K., Martin, S. T., Hanna, S. J., Smith, M. L., Bodsworth, A., Chen, Q., Kuwata,
10 M., Liu, A., You, Y. and Zorn, S. R.: Predicting the relative humidities of liquid-liquid phase
11 separation, efflorescence, and deliquescence of mixed particles of ammonium sulfate, organic
12 material, and water using the organic-to-sulfate mass ratio of the particle and the oxygen-to-
13 carbon elemental ratio of the organic component, *Atmos Chem Phys*, 11(21), 10995–11006,
14 doi:10.5194/acp-11-10995-2011, 2011.
- 15 Budisulistiorini, S. H., Canagaratna, M. R., Croteau, P. L., Marth, W. J., Baumann, K.,
16 Edgerton, E. S., Shaw, S. L., Knipping, E. M., Worsnop, D. R., Jayne, J. T., Gold, A. and
17 Surratt, J. D.: Real-Time Continuous Characterization of Secondary Organic Aerosol Derived
18 from Isoprene Epoxydiols in Downtown Atlanta, Georgia, Using the Aerodyne Aerosol
19 Chemical Speciation Monitor, *Environ. Sci. Technol.*, 47(11), 5686–5694,
20 doi:10.1021/es400023n, 2013.
- 21 Budisulistiorini, S. H., Li, X., Bairai, S. T., Renfro, J., Liu, Y., Liu, Y. J., McKinney, K. A.,
22 Martin, S. T., McNeill, V. F., Pye, H. O. T., Nenes, A., Neff, M. E., Stone, E. A., Mueller, S.,
23 Knote, C., Shaw, S. L., Zhang, Z., Gold, A. and Surratt, J. D.: Examining the effects of
24 anthropogenic emissions on isoprene-derived secondary organic aerosol formation during the
25 2013 Southern Oxidant and Aerosol Study (SOAS) at the Look Rock, Tennessee ground site,
26 *Atmos Chem Phys*, 15(15), 8871–8888, doi:10.5194/acp-15-8871-2015, 2015.
- 27 Carlton, A. G., Wiedinmyer, C. and Kroll, J. H.: A review of Secondary Organic Aerosol
28 (SOA) formation from isoprene, *Atmos Chem Phys*, 9(14), 4987–5005, doi:10.5194/acp-9-
29 4987-2009, 2009.
- 30 Chan, A. W. H., Chan, M. N., Surratt, J. D., Chhabra, P. S., Loza, C. L., Crouse, J. D., Yee,
31 L. D., Flagan, R. C., Wennberg, P. O. and Seinfeld, J. H.: Role of aldehyde chemistry and
32 NO_x concentrations in secondary organic aerosol formation, *Atmos Chem Phys*, 10(15),
33 7169–7188, doi:10.5194/acp-10-7169-2010, 2010a.
- 34 Chan, M. N., Surratt, J. D., Claeys, M., Edgerton, E. S., Tanner, R. L., Shaw, S. L., Zheng,
35 M., Knipping, E. M., Eddingsaas, N. C., Wennberg, P. O. and Seinfeld, J. H.:
36 Characterization and Quantification of Isoprene-Derived Epoxydiols in Ambient Aerosol in
37 the Southeastern United States, *Environ. Sci. Technol.*, 44(12), 4590–4596,
38 doi:10.1021/es100596b, 2010b.
- 39 Chen, Q., Liu, Y., Donahue, N. M., Shilling, J. E. and Martin, S. T.: Particle-Phase Chemistry
40 of Secondary Organic Material: Modeled Compared to Measured O:C and H:C Elemental
41 Ratios Provide Constraints, *Environ. Sci. Technol.*, 45(11), 4763–4770,
42 doi:10.1021/es104398s, 2011.

- 1 Claeys, M., Wang, W., Ion, A. C., Kourtchev, I., Gelencsér, A. and Maenhaut, W.: Formation
2 of secondary organic aerosols from isoprene and its gas-phase oxidation products through
3 reaction with hydrogen peroxide, *Atmos. Environ.*, 38(25), 4093–4098,
4 doi:10.1016/j.atmosenv.2004.06.001, 2004.
- 5 Clegg, S. L., Brimblecombe, P. and Wexler, A. S.: Thermodynamic Model of the System
6 $\text{H}^+ - \text{NH}_4^+ - \text{SO}_4^{2-} - \text{NO}_3^- - \text{H}_2\text{O}$ at Tropospheric Temperatures, *J. Phys. Chem. A*, 102(12),
7 2137–2154, doi:10.1021/jp973042r, 1998.
- 8 Darer, A. I., Cole-Filipiak, N. C., O'Connor, A. E. and Elrod, M. J.: Formation and Stability
9 of Atmospherically Relevant Isoprene-Derived Organosulfates and Organonitrates, *Environ.*
10 *Sci. Technol.*, 45(5), 1895–1902, doi:10.1021/es103797z, 2011.
- 11 Dommen, J., Metzger, A., Duplissy, J., Kalberer, M., Alfarra, M. R., Gascho, A.,
12 Weingartner, E., Prevot, A. S. H., Verheggen, B. and Baltensperger, U.: Laboratory
13 observation of oligomers in the aerosol from isoprene/NO_x photooxidation, *Geophys. Res.*
14 *Lett.*, 33(13), L13805, doi:10.1029/2006GL026523, 2006.
- 15 Eddingsaas, N. C., VanderVelde, D. G. and Wennberg, P. O.: Kinetics and Products of the
16 Acid-Catalyzed Ring-Opening of Atmospherically Relevant Butyl Epoxy Alcohols, *J. Phys.*
17 *Chem. A*, 114(31), 8106–8113, doi:10.1021/jp103907c, 2010.
- 18 Eddingsaas, N. C., Loza, C. L., Yee, L. D., Chan, M., Schilling, K. A., Chhabra, P. S.,
19 Seinfeld, J. H. and Wennberg, P. O.: α -pinene photooxidation under controlled chemical
20 conditions-Part 2: SOA yield and composition in low- and high-NO_x environments,
21 *Atmospheric Chem. Phys.*, 12(16), 7413–7427, doi:10.5194/acp-12-7413-2012, 2012.
- 22 Edney, E. O., Kleindienst, T. E., Jaoui, M., Lewandowski, M., Offenberg, J. H., Wang, W.
23 and Claeys, M.: Formation of 2-methyl tetrols and 2-methylglyceric acid in secondary organic
24 aerosol from laboratory irradiated isoprene/NO_x/SO₂/air mixtures and their detection in
25 ambient PM_{2.5} samples collected in the eastern United States, *Atmos. Environ.*, 39(29),
26 5281–5289, doi:10.1016/j.atmosenv.2005.05.031, 2005.
- 27 Finlayson-Pitts, B. J. and Pitts, Jr., J. N.: Atmospheric Chemistry of Tropospheric Ozone
28 Formation: Scientific and Regulatory Implications, *J. Air Waste Assoc.*, 43(8), 1091–1100,
29 doi:10.1080/1073161X.1993.10467187, 1993.
- 30 Gaston, C. J., Riedel, T. P., Zhang, Z., Gold, A., Surratt, J. D. and Thornton, J. A.: Reactive
31 Uptake of an Isoprene-Derived Epoxydiol to Submicron Aerosol Particles, *Environ. Sci.*
32 *Technol.*, 48(19), 11178–11186, doi:10.1021/es5034266, 2014.
- 33 Guenther, A., Karl, T., Harley, P., Wiedinmyer, C., Palmer, P. I. and Geron, C.: Estimates of
34 global terrestrial isoprene emissions using MEGAN (Model of Emissions of Gases and
35 Aerosols from Nature), *Atmos Chem Phys*, 6(11), 3181–3210, doi:10.5194/acp-6-3181-2006,
36 2006.
- 37 Guo, H., Xu, L., Bougiatioti, A., Cerully, K. M., Capps, S. L., Hite, J. R., Carlton, A. G., Lee,
38 S.-H., Bergin, M. H., Ng, N. L., Nenes, A. and Weber, R. J.: Fine-particle water and pH in the
39 southeastern United States, *Atmospheric Chem. Phys.*, 15(9), 5211–5228, doi:10.5194/acp-
40 15-5211-2015, 2015.

- 1 Heintzenberg, J.: Fine particles in the global troposphere A review, *Tellus B*, 41B(2), 149–
2 160, doi:10.1111/j.1600-0889.1989.tb00132.x, 1989.
- 3 Hennigan, C. J., Bergin, M. H., Dibb, J. E. and Weber, R. J.: Enhanced secondary organic
4 aerosol formation due to water uptake by fine particles, *Geophys. Res. Lett.*, 35(18), L18801,
5 doi:10.1029/2008GL035046, 2008.
- 6 Henze, D. K. and Seinfeld, J. H.: Global secondary organic aerosol from isoprene oxidation,
7 *Geophys. Res. Lett.*, 33(9), L09812, doi:10.1029/2006GL025976, 2006.
- 8 Hodas, N., Zuend, A., Mui, W., Flagan, R. C. and Seinfeld, J. H.: Influence of particle-phase
9 state on the hygroscopic behavior of mixed organic–inorganic aerosols, *Atmos Chem Phys*,
10 15(9), 5027–5045, doi:10.5194/acp-15-5027-2015, 2015.
- 11 Im, Y., Jang, M. and Beardsley, R. L.: Simulation of aromatic SOA formation using the
12 lumping model integrated with explicit gas-phase kinetic mechanisms and aerosol-phase
13 reactions, *Atmos Chem Phys*, 14(8), 4013–4027, doi:10.5194/acp-14-4013-2014, 2014.
- 14 Ip, H. S. S., Huang, X. H. H. and Yu, J. Z.: Effective Henry’s law constants of glyoxal,
15 glyoxylic acid, and glycolic acid, *Geophys. Res. Lett.*, 36(1), L01802,
16 doi:10.1029/2008GL036212, 2009.
- 17 Jang, M. and Kamens, R. M.: A Thermodynamic Approach for Modeling Partitioning of
18 Semivolatile Organic Compounds on Atmospheric Particulate Matter: Humidity Effects,
19 *Environ. Sci. Technol.*, 32, 1237–1243, doi:10.1021/es970773w, 1998.
- 20 Jang, M. and Kamens, R. M.: Characterization of Secondary Aerosol from the Photooxidation
21 of Toluene in the Presence of NO_x and 1-Propene, *Environ. Sci. Technol.*, 35, 3626–3639,
22 doi:10.1021/es010676+, 2001.
- 23 Jang, M., Czoschke, N. M., Lee, S. and Kamens, R. M.: Heterogeneous Atmospheric Aerosol
24 Production by Acid-Catalyzed Particle-Phase Reactions, *Science*, 298(5594), 814–817,
25 doi:10.1126/science.1075798, 2002.
- 26 Jang, M., Carroll, B., Chandramouli, B. and Kamens, R. M.: Particle Growth by Acid-
27 Catalyzed Heterogeneous Reactions of Organic Carbonyls on Preexisting Aerosols, *Environ.*
28 *Sci. Technol.*, 37(17), 3828–3837, doi:10.1021/es021005u, 2003.
- 29 Jang, M., Czoschke, N. M. and Northcross, A. L.: Semiempirical Model for Organic Aerosol
30 Growth by Acid-Catalyzed Heterogeneous Reactions of Organic Carbonyls, *Environ. Sci.*
31 *Technol.*, 39(1), 164–174, doi:10.1021/es048977h, 2005.
- 32 Jang, M., Czoschke, N. M., Northcross, A. L., Cao, G. and Shaof, D.: SOA Formation from
33 Partitioning and Heterogeneous Reactions: Model Study in the Presence of Inorganic
34 Species, *Environ. Sci. Technol.*, 40(9), 3013–3022, doi:10.1021/es0511220, 2006.
- 35 Jang, M., Cao, G. and Paul, J.: Colorimetric Particle Acidity Analysis of Secondary Organic
36 Aerosol Coating on Submicron Acidic Aerosols, *Aerosol Sci. Technol.*, 42(6), 409–420,
37 doi:10.1080/02786820802154861, 2008.

- 1 Jeffries, H.E., Gary, M. W., Kessler, M and Sexton, K. G.: Morphecule reaction mechanism,
2 Morpho., 1998.
- 3 Joback, K. G. and Reid, R. C.: Estimation of Pure-Component Properties from Group-
4 Contributions, Chem. Eng. Commun., 57(1-6), 233–243, doi:10.1080/00986448708960487,
5 1987.
- 6 Kleindienst, T. E., Jaoui, M., Lewandowski, M., Offenber, J. H., Lewis, C. W., Bhave, P. V.
7 and Edney, E. O.: Estimates of the contributions of biogenic and anthropogenic hydrocarbons
8 to secondary organic aerosol at a southeastern US location, Atmos. Environ., 41(37), 8288–
9 8300, doi:10.1016/j.atmosenv.2007.06.045, 2007.
- 10 Kolská, Z., Růžička, V. and Gani, R.: Estimation of the Enthalpy of Vaporization and the
11 Entropy of Vaporization for Pure Organic Compounds at 298.15 K and at Normal Boiling
12 Temperature by a Group Contribution Method, Ind. Eng. Chem. Res., 44(22), 8436–8454,
13 doi:10.1021/ie050113x, 2005.
- 14 Kroll, J. H., Ng, N. L., Murphy, S. M., Flagan, R. C. and Seinfeld, J. H.: Secondary organic
15 aerosol formation from isoprene photooxidation under high-NO_x conditions, Geophys. Res.
16 Lett., 32(18), L18808, doi:10.1029/2005GL023637, 2005.
- 17 Kroll, J. H., Ng, N. L., Murphy, S. M., Flagan, R. C. and Seinfeld, J. H.: Secondary Organic
18 Aerosol Formation from Isoprene Photooxidation, Environ. Sci. Technol., 40(6), 1869–1877,
19 doi:10.1021/es0524301, 2006.
- 20 Kuwata, M., Shao, W., Lebouteiller, R. and Martin, S. T.: Classifying organic materials by
21 oxygen-to-carbon elemental ratio to predict the activation regime of Cloud Condensation
22 Nuclei (CCN), Atmospheric Chem. Phys., 13(10), 5309–5324, doi:10.5194/acp-13-5309-
23 2013, 2013.
- 24 Kuwata, M., Liu, Y., McKinney, K. and Martin, S. T.: Physical state and acidity of inorganic
25 sulfate can regulate the production of secondary organic material from isoprene
26 photooxidation products, Phys. Chem. Chem. Phys., 17(8), 5670–5678,
27 doi:10.1039/C4CP04942J, 2015.
- 28 Lewandowski, M., Jaoui, M., Offenber, J. H., Krug, J. D. and Kleindienst, T. E.:
29 Atmospheric oxidation of isoprene and 1,3-butadiene: influence of aerosol acidity and relative
30 humidity on secondary organic aerosol, Atmos Chem Phys, 15(7), 3773–3783,
31 doi:10.5194/acp-15-3773-2015, 2015.
- 32 Liao, J., Froyd, K. D., Murphy, D. M., Keutsch, F. N., Yu, G., Wennberg, P. O., St. Clair, J.
33 M., Crouse, J. D., Wisthaler, A., Mikoviny, T., Jimenez, J. L., Campuzano-Jost, P., Day, D.
34 A., Hu, W., Ryerson, T. B., Pollack, I. B., Peischl, J., Anderson, B. E., Ziemba, L. D., Blake,
35 D. R., Meinardi, S. and Diskin, G.: Airborne measurements of organosulfates over the
36 continental U.S., J. Geophys. Res. Atmospheres, 120(7), 2014JD022378,
37 doi:10.1002/2014JD022378, 2015.
- 38 Liggió, J., Li, S.-M. and McLaren, R.: Heterogeneous Reactions of Glyoxal on Particulate
39 Matter: Identification of Acetals and Sulfate Esters, Environ. Sci. Technol., 39, 1532–1541,
40 doi:10.1021/es048375y, 2005.

- 1 Li, J. and Jang, M.: Aerosol Acidity Measurement Using Colorimetry Coupled With a
2 Reflectance UV-Visible Spectrometer, *Aerosol Sci. Technol.*, 46(8), 833–842,
3 doi:10.1080/02786826.2012.669873, 2012.
- 4 Li, J., Jang, M. and Beardsley, R. L.: Dialkylsulfate formation in sulfuric acid-seeded
5 secondary organic aerosol produced using an outdoor chamber under natural sunlight,
6 *Environ. Chem.*, doi:10.1071/EN15129, 2015.
- 7 Limbeck, A., Kulmala, M. and Puxbaum, H.: Secondary organic aerosol formation in the
8 atmosphere via heterogeneous reaction of gaseous isoprene on acidic particles, *Geophys. Res.*
9 *Lett.*, 30(19), 1996, doi:10.1029/2003GL017738, 2003.
- 10 Lim, Y. B., Tan, Y., Perri, M. J., Seitzinger, S. P. and Turpin, B. J.: Aqueous chemistry and
11 its role in secondary organic aerosol (SOA) formation, *Atmospheric Chem. Phys.*, 10(21),
12 10521–10539, doi:10.5194/acp-10-10521-2010, 2010.
- 13 Lin, Y.-H., Zhang, Z., Docherty, K. S., Zhang, H., Budisulistiorini, S. H., Rubitschun, C. L.,
14 Shaw, S. L., Knipping, E. M., Edgerton, E. S., Kleindienst, T. E., Gold, A. and Surratt, J. D.:
15 Isoprene Epoxydiols as Precursors to Secondary Organic Aerosol Formation: Acid-Catalyzed
16 Reactive Uptake Studies with Authentic Compounds, *Environ. Sci. Technol.*, 46(1), 250–258,
17 doi:10.1021/es202554c, 2012.
- 18 Marais, E. A., Jacob, D. J., Jimenez, J. L., Campuzano-Jost, P., Day, D. A., Hu, W.,
19 Krechmer, J., Zhu, L., Kim, P. S., Miller, C. C., Fisher, J. A., Travis, K., Yu, K., Hanisco, T.
20 F., Wolfe, G. M., Arkinson, H. L., Pye, H. O. T., Froyd, K. D., Liao, J. and McNeill, V. F.:
21 Aqueous-phase mechanism for secondary organic aerosol formation from isoprene:
22 application to the southeast United States and co-benefit of SO₂ emission controls, *Atmos*
23 *Chem Phys*, 16(3), 1603–1618, doi:10.5194/acp-16-1603-2016, 2016.
- 24 Matsunaga, A. and Ziemann, P. J.: Gas-Wall Partitioning of Organic Compounds in a Teflon
25 Film Chamber and Potential Effects on Reaction Product and Aerosol Yield Measurements,
26 *Aerosol Sci. Technol.*, 44(10), 881–892, doi:10.1080/02786826.2010.501044, 2010.
- 27 McNeill, V. F., Woo, J. L., Kim, D. D., Schwier, A. N., Wannell, N. J., Sumner, A. J. and
28 Barakat, J. M.: Aqueous-Phase Secondary Organic Aerosol and Organosulfate Formation in
29 Atmospheric Aerosols: A Modeling Study, *Environ. Sci. Technol.*, 46(15), 8075–8081,
30 doi:10.1021/es3002986, 2012.
- 31 Minerath, E. C., Casale, M. T. and Elrod, M. J.: Kinetics Feasibility Study of Alcohol Sulfate
32 Esterification Reactions in Tropospheric Aerosols, *Environ. Sci. Technol.*, 42(12), 4410–
33 4415, doi:10.1021/es8004333, 2008.
- 34 Murphy, D. M., Cziczo, D. J., Froyd, K. D., Hudson, P. K., Matthew, B. M., Middlebrook, A.
35 M., Peltier, R. E., Sullivan, A., Thomson, D. S. and Weber, R. J.: Single-particle mass
36 spectrometry of tropospheric aerosol particles, *J. Geophys. Res. Atmospheres*, 111(D23),
37 D23S32, doi:10.1029/2006JD007340, 2006.
- 38 Ng, N. L., Kwan, A. J., Surratt, J. D., Chan, A. W. H., Chhabra, P. S., Sorooshian, A., Pye, H.
39 O. T., Crouse, J. D., Wennberg, P. O., Flagan, R. C. and Seinfeld, J. H.: Secondary organic
40 aerosol (SOA) formation from reaction of isoprene with nitrate radicals (NO₃), *Atmospheric*
41 *Chem. Phys.*, 8, 4117–4140, doi:10.5194/acp-8-4117-2008, 2008.

- 1 Nguyen, T. B., Bateman, A. P., Bones, D. L., Nizkorodov, S. A., Laskin, J. and Laskin, A.:
2 High-resolution mass spectrometry analysis of secondary organic aerosol generated by
3 ozonolysis of isoprene, *Atmos. Environ.*, 44(8), 1032–1042,
4 doi:10.1016/j.atmosenv.2009.12.019, 2010.
- 5 Nguyen, T. B., Roach, P. J., Laskin, J., Laskin, A. and Nizkorodov, S. A.: Effect of humidity
6 on the composition of isoprene photooxidation secondary organic aerosol, *Atmos Chem Phys*,
7 11(14), 6931–6944, doi:10.5194/acp-11-6931-2011, 2011.
- 8 Odum, J. R., Hoffman, T., Bowman, F., Collins, D., Flagan, R. C. and Seinfeld, J. H.:
9 Gas/Particle Partitioning and Secondary Organic Aerosol Yields, *Environ. Sci. Technol.*,
10 30(8), 2580–2585, 1996.
- 11 Pandis, S. N., Paulson, S. E., Seinfeld, J. H. and Flagan, R. C.: Aerosol formation in the
12 photooxidation of isoprene and β -pinene, *Atmospheric Environ. Part Gen. Top.*, 25(5–6),
13 997–1008, doi:10.1016/0960-1686(91)90141-S, 1991.
- 14 Pankow, J. F.: An absorption model of gas/particle partitioning of organic compounds in the
15 atmosphere, *Atmos. Environ.*, 28(2), 185–188, doi:10.1016/1352-2310(94)90093-0, 1994.
- 16 Paulot, F., Crounse, J. D., Kjaergaard, H. G., Kürten, A., Clair, J. M. S., Seinfeld, J. H. and
17 Wennberg, P. O.: Unexpected Epoxide Formation in the Gas-Phase Photooxidation of
18 Isoprene, *Science*, 325(5941), 730–733, doi:10.1126/science.1172910, 2009.
- 19 Pinho, P. G., Pio, C. A. and Jenkin, M. E.: Evaluation of isoprene degradation in the detailed
20 tropospheric chemical mechanism, MCM v3, using environmental chamber data, *Atmos.*
21 *Environ.*, 39(7), 1303–1322, doi:10.1016/j.atmosenv.2004.11.014, 2005.
- 22 Pye, H. O. T., Pinder, R. W., Piletic, I. R., Xie, Y., Capps, S. L., Lin, Y.-H., Surratt, J. D.,
23 Zhang, Z., Gold, A., Luecken, D. J., Hutzell, W. T., Jaoui, M., Offenberg, J. H., Kleindienst,
24 T. E., Lewandowski, M. and Edney, E. O.: Epoxide Pathways Improve Model Predictions of
25 Isoprene Markers and Reveal Key Role of Acidity in Aerosol Formation, *Environ. Sci.*
26 *Technol.*, 47(19), 11056–11064, doi:10.1021/es402106h, 2013.
- 27 R. M. Kamens, M. W. Gery, H. E. Jeffries, M. Jackson and E. I. Cole: Ozone-isoprene
28 reactions: Product formation and aerosol potential, *Int. J. Chem. Kinet. - INT J CHEM*
29 *KINET*, 14(9), 955–975, doi:10.1002/kin.550140902, 1982.
- 30 Rollins, A. W., Browne, E. C., Min, K.-E., Pusede, S. E., Wooldridge, P. J., Gentner, D. R.,
31 Goldstein, A. H., Liu, S., Day, D. A., Russell, L. M. and Cohen, R. C.: Evidence for NO_x
32 Control over Nighttime SOA Formation, *Science*, 337(6099), 1210–1212,
33 doi:10.1126/science.1221520, 2012.
- 34 Saunders, S. M., Jenkin, M. E., Derwent, R. G. and Pilling, M. J.: World wide web site of a
35 master chemical mechanism (MCM) for use in tropospheric chemistry models, *Atmospheric*
36 *Environ. - ATMOS Env.*, 31(8), 1249–1249, doi:10.1016/S1352-2310(97)85197-7, 1997.
- 37 Saunders, S. M., Jenkin, M. E., Derwent, R. G. and Pilling, M. J.: Protocol for the
38 development of the Master Chemical Mechanism, MCM v3 (Part A): tropospheric
39 degradation of non-aromatic volatile organic compounds, *Atmos Chem Phys*, 3(1), 161–180,
40 doi:10.5194/acp-3-161-2003, 2003.

- 1 Schell, B., Ackermann, I. J., Hass, H., Binkowski, F. S. and Ebel, A.: Modeling the formation
2 of secondary organic aerosol within a comprehensive air quality model system, *J. Geophys.*
3 *Res. Atmospheres*, 106(D22), 28275–28293, doi:10.1029/2001JD000384, 2001.
- 4 Song, M., Liu, P. F., Hanna, S. J., Li, Y. J., Martin, S. T. and Bertram, A. K.: Relative
5 humidity-dependent viscosities of isoprene-derived secondary organic material and
6 atmospheric implications for isoprene-dominant forests, *Atmos Chem Phys*, 15(9), 5145–
7 5159, doi:10.5194/acp-15-5145-2015, 2015.
- 8 Stein, S. E. and Brown, R. L.: Estimation of normal boiling points from group contributions,
9 *J. Chem. Inf. Model.*, 34(3), 581–587, doi:10.1021/ci00019a016, 1994.
- 10 Surratt, J. D., Murphy, S. M., Kroll, J. H., Ng, N. L., Hildebrandt, L., Sorooshian, A.,
11 Szmigielski, R., Vermeylen, R., Maenhaut, W., Claeys, M., Flagan, R. C. and Seinfeld, J. H.:
12 Chemical composition of secondary organic aerosol formed from the photooxidation of
13 isoprene, *J. Phys. Chem. A*, 110(31), 9665–9690, doi:10.1021/jp061734m, 2006.
- 14 Surratt, J. D., Lewandowski, M., Offenberg, J. H., Jaoui, M., Kleindienst, T. E., Edney, E. O.
15 and Seinfeld, J. H.: Effect of Acidity on Secondary Organic Aerosol Formation from
16 Isoprene, *Environ. Sci. Technol.*, 41(15), 5363–5369, doi:10.1021/es0704176, 2007.
- 17 Surratt, J. D., Chan, A. W. H., Eddingsaas, N. C., Chan, M., Loza, C. L., Kwan, A. J., Hersey,
18 S. P., Flagan, R. C., Wennberg, P. O. and Seinfeld, J. H.: Reactive intermediates revealed in
19 secondary organic aerosol formation from isoprene, *Proc. Natl. Acad. Sci. U. S. A.*, 107(15),
20 6640–6645, doi:10.1073/pnas.0911114107, 2010.
- 21 Virtanen, A., Joutsensaari, J., Koop, T., Kannosto, J., Yli-Pirilä, P., Leskinen, J., Mäkelä, J.
22 M., Holopainen, J. K., Pöschl, U., Kulmala, M., Worsnop, D. R. and Laaksonen, A.: An
23 amorphous solid state of biogenic secondary organic aerosol particles, *Nature*, 467(7317),
24 824–827, doi:10.1038/nature09455, 2010.
- 25 Volkamer, R., San Martini, F., Molina, L. T., Salcedo, D., Jimenez, J. L. and Molina, M. J.: A
26 missing sink for gas-phase glyoxal in Mexico City: Formation of secondary organic aerosol,
27 *Geophys. Res. Lett.*, 34(19), L19807, doi:10.1029/2007GL030752, 2007.
- 28 Waxman, E. M., Elm, J., Kurtén, T., Mikkelsen, K. V., Ziemann, P. J. and Volkamer, R.:
29 Glyoxal and Methylglyoxal Setschenow Salting Constants in Sulfate, Nitrate, and Chloride
30 Solutions: Measurements and Gibbs Energies, *Environ. Sci. Technol.*, 49(19), 11500–11508,
31 doi:10.1021/acs.est.5b02782, 2015.
- 32 Wiedinmyer, C., Friedfeld, S., Baugh, W., Greenberg, J., Guenther, A., Fraser, M. and Allen,
33 D.: Measurement and analysis of atmospheric concentrations of isoprene and its reaction
34 products in central Texas, *Atmos. Environ.*, 35(6), 1001–1013, doi:10.1016/S1352-
35 2310(00)00406-4, 2001.
- 36 Woo, J. L. and McNeill, V. F.: simpleGAMMA v1.0 – a reduced model of secondary organic
37 aerosol formation in the aqueous aerosol phase (aaSOA), *Geosci. Model Dev.*, 8(6), 1821–
38 1829, doi:10.5194/gmd-8-1821-2015, 2015.

- 1 Xu, L., Kollman, M. S., Song, C., Shilling, J. E. and Ng, N. L.: Effects of NO_x on the
2 Volatility of Secondary Organic Aerosol from Isoprene Photooxidation, *Environ. Sci.*
3 *Technol.*, 48(4), 2253–2262, doi:10.1021/es404842g, 2014.
- 4 Xu, L., Guo, H., Boyd, C. M., Klein, M., Bougiatioti, A., Cerully, K. M., Hite, J. R.,
5 Isaacman-VanWertz, G., Kreisberg, N. M., Knote, C., Olson, K., Koss, A., Goldstein, A. H.,
6 Hering, S. V., Gouw, J. de, Baumann, K., Lee, S.-H., Nenes, A., Weber, R. J. and Ng, N. L.:
7 Effects of anthropogenic emissions on aerosol formation from isoprene and monoterpenes in
8 the southeastern United States, *Proc. Natl. Acad. Sci.*, 112(1), 37–42,
9 doi:10.1073/pnas.1417609112, 2015.
- 10 Zhang, H., Worton, D. R., Lewandowski, M., Ortega, J., Rubitschun, C. L., Park, J.-H.,
11 Kristensen, K., Campuzano-Jost, P., Day, D. A., Jimenez, J. L., Jaoui, M., Offenberg, J. H.,
12 Kleindienst, T. E., Gilman, J., Kuster, W. C., de Gouw, J., Park, C., Schade, G. W., Frossard,
13 A. A., Russell, L., Kaser, L., Jud, W., Hansel, A., Cappellin, L., Karl, T., Glasius, M.,
14 Guenther, A., Goldstein, A. H., Seinfeld, J. H., Gold, A., Kamens, R. M. and Surratt, J. D.:
15 Organosulfates as Tracers for Secondary Organic Aerosol (SOA) Formation from 2-Methyl-
16 3-Buten-2-ol (MBO) in the Atmosphere, *Environ. Sci. Technol.*, 46(17), 9437–9446,
17 doi:10.1021/es301648z, 2012.
- 18 Zhang, X., Cappa, C. D., Jathar, S. H., McVay, R. C., Ensberg, J. J., Kleeman, M. J. and
19 Seinfeld, J. H.: Influence of vapor wall loss in laboratory chambers on yields of secondary
20 organic aerosol, *Proc. Natl. Acad. Sci.*, 111(16), 5802–5807, doi:10.1073/pnas.1404727111,
21 2014.
- 22 Zhang, X., McVay, R. C., Huang, D. D., Dalleska, N. F., Aumont, B., Flagan, R. C. and
23 Seinfeld, J. H.: Formation and evolution of molecular products in α -pinene secondary organic
24 aerosol, *Proc. Natl. Acad. Sci.*, 112(46), 14168–14173, doi:10.1073/pnas.1517742112, 2015.
- 25 Zhang, Y., Seigneur, C., Seinfeld, J. H., Jacobson, M., Clegg, S. L. and Binkowski, F. S.: A
26 comparative review of inorganic aerosol thermodynamic equilibrium modules: similarities,
27 differences, and their likely causes, *Atmos. Environ.*, 34(1), 117–137, doi:10.1016/S1352-
28 2310(99)00236-8, 2000.
- 29 Zhao, L., Li, P. and Yalkowsky, S. H.: Predicting the Entropy of Boiling for Organic
30 Compounds, *J. Chem. Inf. Model.*, 39(6), 1112–1116, doi:10.1021/ci990054w, 1999.

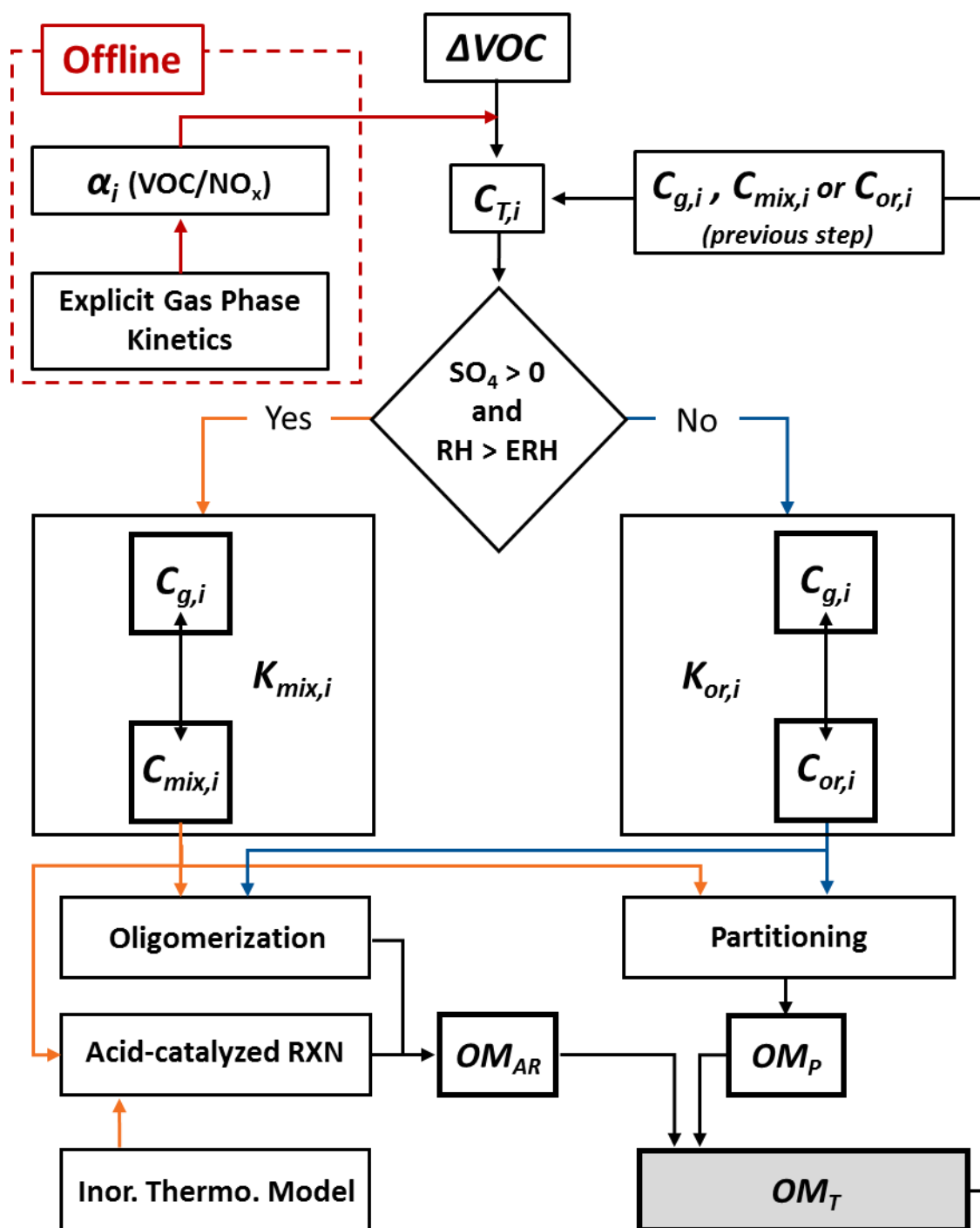
31

32

1 Table 1. Experimental conditions and resulting SOA data of the isoprene photooxidation
 2 experiments performed with and without inorganic acidic seed in the dual, outdoor UF
 3 APHOR chambers. ^a SOA yield ($Y_{SOA} = \Delta OM / \Delta Iso$) is calculated at the point of maximum
 4 organic mass (OM). ^b In Exp. SO2, SO₂ (g) was injected into the chamber to generate acidic
 5 seeds instead of directly injecting H₂SO₄ (aq).

Exp.	Date	RH (%)	Temp (K)	[ISO]₀ (ppb)	[NO_x]₀ (ppb)	VOC/NO_x (ppbC/ppb)	[H₂SO₄] (μg m⁻³)	Y_{SOA}^a (%)
ISO1	2015-01-27	27-66	279-298	839	241	17.4	0	2.5
SA1	2015-01-27	20-54	279-299	850	253	16.8	53	8.5
ISO2	2014-12-14	19-49	282-303	852	131	32.7	0	0.7
SA2	2014-12-14	14-40	284-305	857	130	32.5	40	4.8
SO2	2014-01-18	48-91	273-292	627	91	34.6	26 ^b	3.0

6
 7
 8
 9
 10



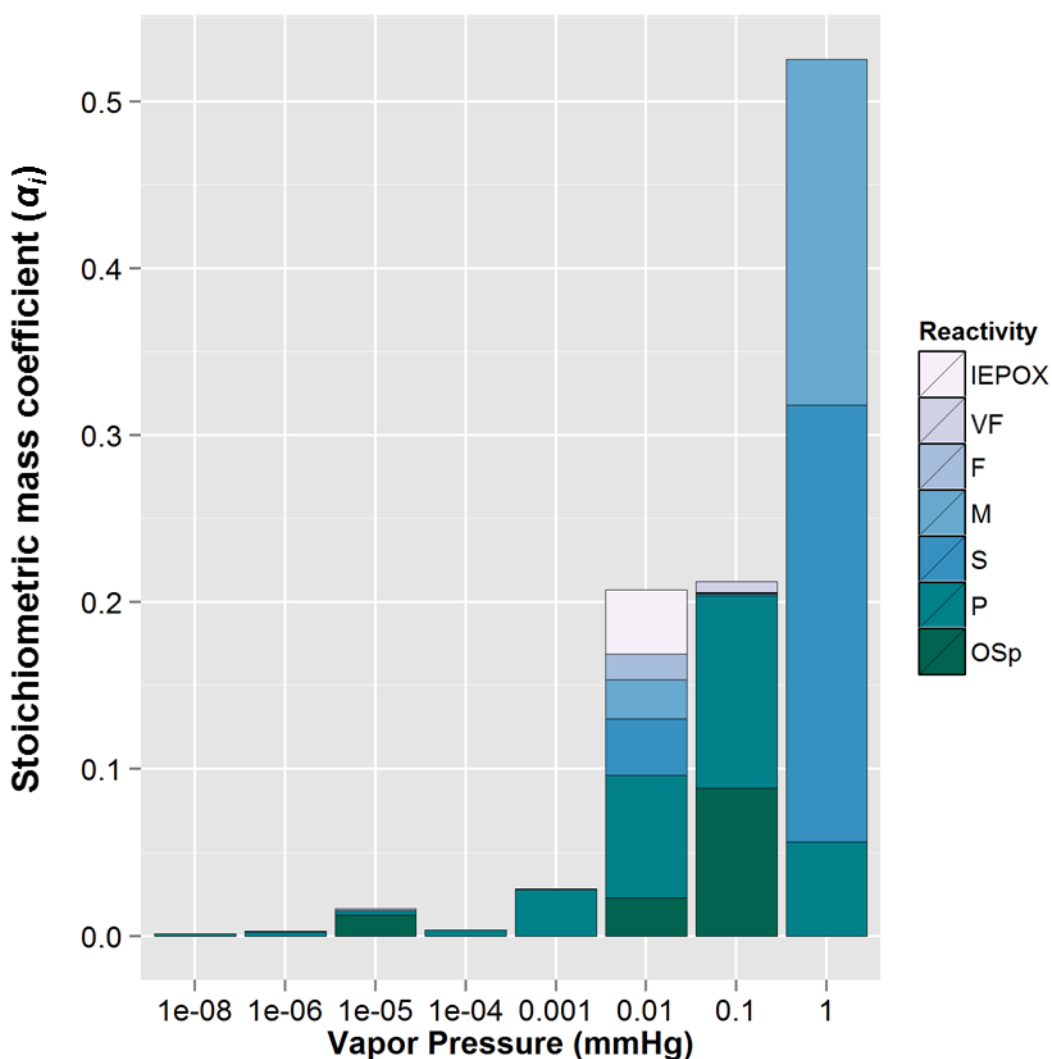
1
2

3 Figure 1. The overall schematic of the model applied to simulate isoprene SOA within
 4 UNIPAR. $C_{T,i}$ is the total concentration of each lumping species, i , and $C_{g,i}$, $C_{\text{mix},i}$, and $C_{\text{or},i}$ are
 5 the concentrations of each i within the gas, single homogeneously mixed (SHMP) aerosol, and
 6 organic-only aerosol, respectively. ΔVOC is the consumption of the volatile organic compound
 7 of interest in each time step. α_i is the stoichiometric mass ratio of each i , which is calculated

1 offline as a function of VOC/NO_x based on explicit gas phase simulations, and is used to
2 distribute the total Δ VOC between each i . $K_{\text{mix},i}$ and $K_{\text{or},i}$ are the equilibrium partitioning
3 coefficients for the SHMP and organic-only aerosol, respectively. OM_T , OM_P and OM_{AR} are
4 the total organic mass and the organic mass from aerosol phase reactions and partitioning,
5 respectively.

6

7

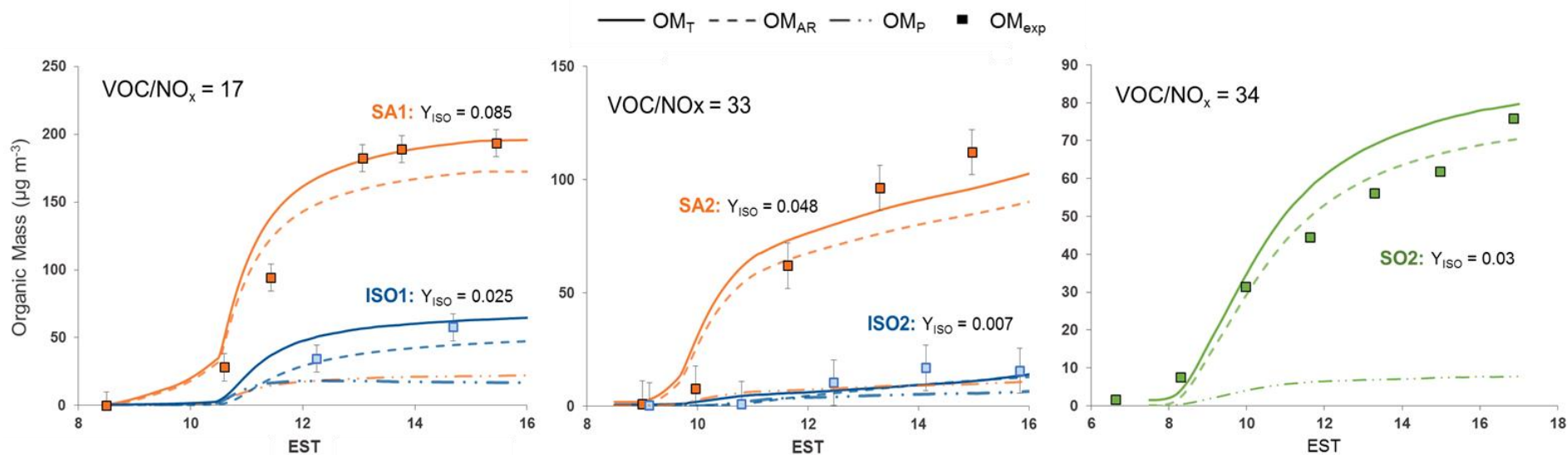


1

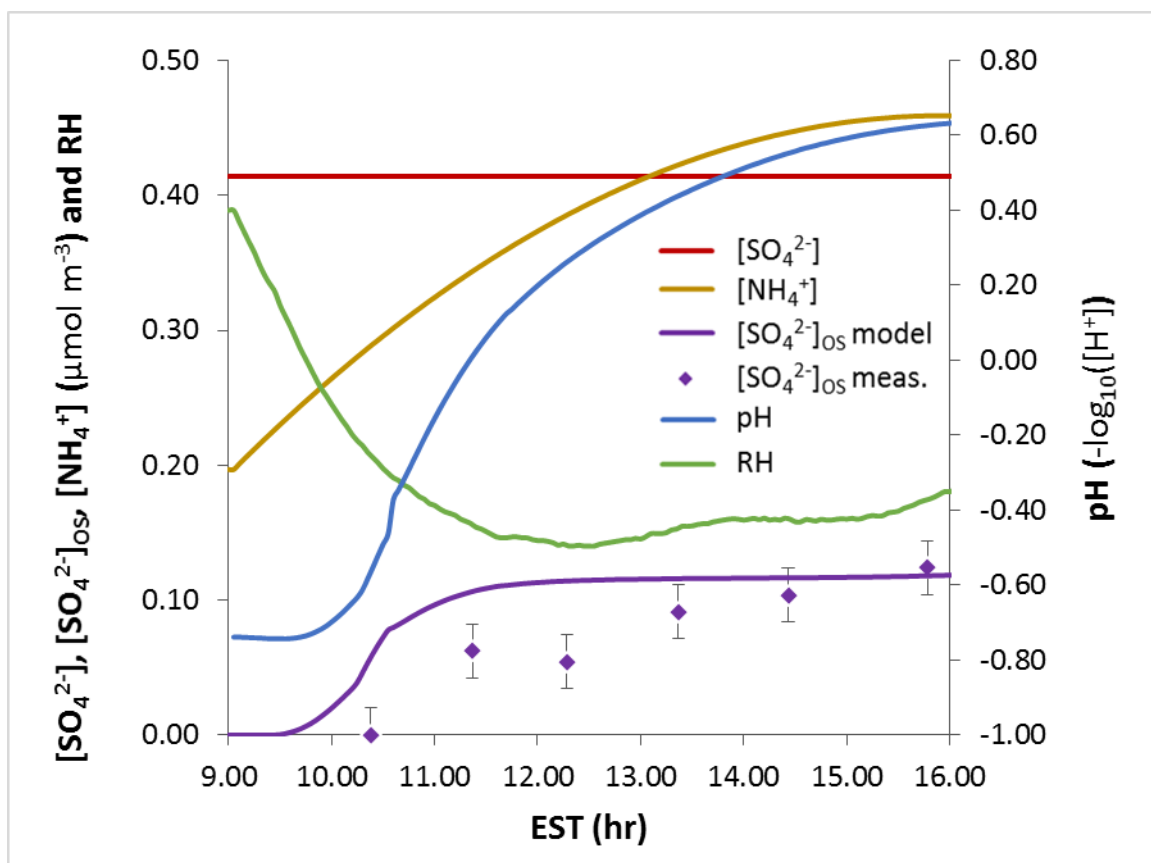
2

3 Figure 2. The stoichiometric mass coefficients (α_i) of each lumping group at a VOC/NO_x
 4 (ppbC/ppb) of 25. The photooxidation products predicted by an explicit gas phase chemical
 5 mechanism are lumped as a function of vapor pressure (x-axis, 8 bins) and aerosol phase
 6 reactivity (y-axis, 6 bins). The aerosol phase reactivity bins are very fast (VF, α -
 7 hydroxybicycbonyls and tricycbonyls), fast (F, 2 epoxides or aldehydes,), medium (M, 1
 8 epoxide or aldehyde), slow (S, ketones), partitioning only (P), organosulfate precursors (OS_P,
 9 3 or more alcohols) and IEPOX products, which were lumped separately to more easily
 10 quantify their contribution.

1



2 Figure 3. Time profiles of the experimentally measured and simulated SOA mass concentrations resulting from the photooxidation of
 3 isoprene. Data from experiments performed in the absence of inorganic seed is shown in blue, in the presence of sulfuric acid in orange, and
 4 in the presence of inorganic seed generated from SO_2 photooxidation in green. Solid, dashed, and dashed-dotted lines represent the simulated
 5 total organic mass (OM_T), organic mass from aerosol phase reactions (OM_{AR}), and organic mass from partitioning (OM_P), respectively. The
 6 experimental measured organic mass (OM_{exp}) is shown with square markers and is corrected for particle wall loss. The VOC/NO_x (ppbC/ppb)
 7 are shown for each experiment.



1
 2 Figure 4. Time profiles of the total inorganic sulfate ($[\text{SO}_4^{2-}]$) and ammonium ($[\text{NH}_4^+]$)
 3 concentrations, and RH from Experiment SA2, along with the measured and model predicted
 4 concentrations of the sulfate associated with organosulfates (OS) ($[\text{SO}_4^{2-}]_{\text{os}}$), and the
 5 predicted particle pH.

6
 7
 8
 9 \\
 10
 11
 12
 13
 14
 15

1
2
3
4
5
6
7
8
9
10
11
12
13
14
15
16
17
18
19
20
21
22
23
24

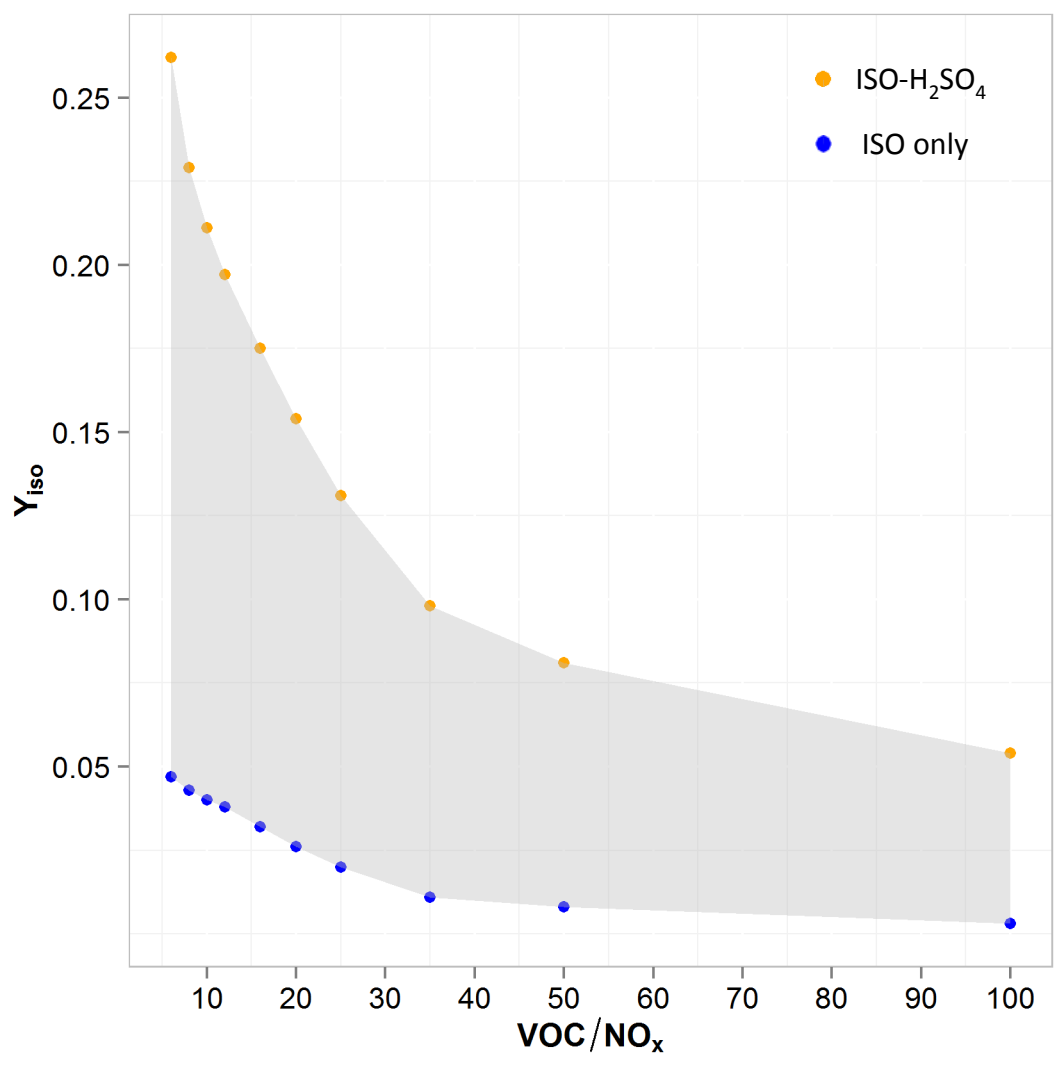
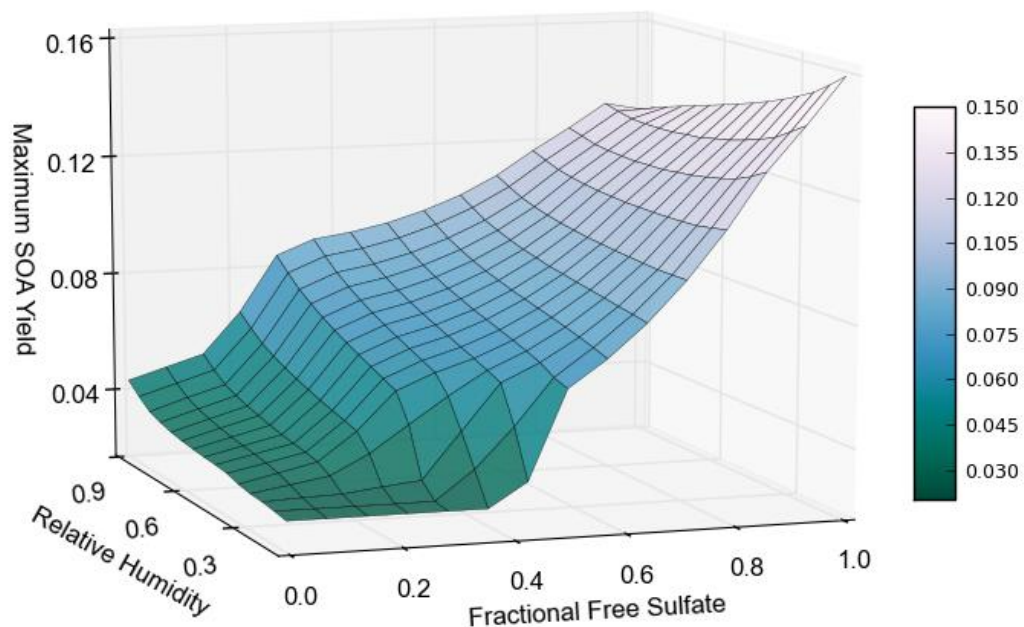


Figure 5. Simulated isoprene SOA yields ($Y_{SOA} = \Delta OM / \Delta Iso$) as a function of VOC/NO_x (ppbC/ppb) for values 10 to 100. The simulations were performed using the experimental conditions of SA1 (Table 1) without inorganic seed (blue) and in the presence of untitrated sulfuric acid (orange).

Maximum Isoprene SOA Yield



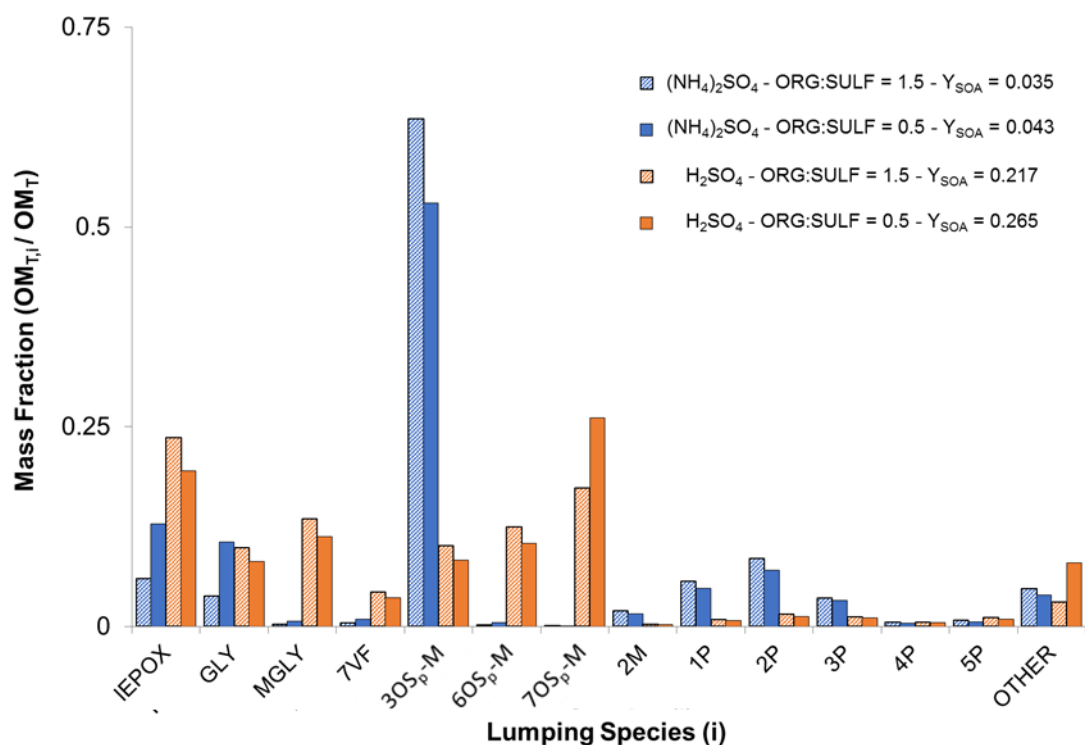
1

2

3 Figure 6. Simulated isoprene SOA yields ($Y_{SOA} = \Delta OM / \Delta Iso$) as a function of relative
4 humidity (RH) and fractional free sulfate (FFS = $([SO_4^{2-}] - 0.5[NH_4^+]) / [SO_4^{2-}]$). Using the
5 experimental conditions of SA1, the RH and FFS were varied to determine the impact of
6 acidity and aerosol liquid water content on Y_{SOA} .

7

8



1
2
3
4
5
6
7
8
9

Figure 7. The mass fraction ($MF_i = OM_{T,i} / OM_T$) of each lumping species, i , that contribute significantly to the simulated isoprene SOA in the presence of ammonium sulfate, $(NH_4)_2SO_4$, and sulfuric acid seeds, H_2SO_4 , at organic to sulfur mass ratios of 0.5 and 1.5. The MF_i of the remaining lumping groups are summed and included in 'OTHER.' The MF_i , Y_{SOA} , and org:sulf are calculated at the point of maximum SOA mass with an initial VOC/ NO_x ratio of ~17 (Exp. SA1 in Table 1).